JOURNAL OF PETROLOGY | VOLUME 53 | NUMBER 1 | PAGES 127–157 | 2012 | doi:10.1093/petrology/egr059

Melting of a Two-component Source beneath Iceland

J. M. KOORNNEEF[1]*, A. STRACKE[1,†], B. BOURDON[1,††], M. A. MEIER[1], K. P. JOCHUM[2], B. STOLL[2] AND K. GRÖNVOLD[3]

[1]INSTITUTE OF GEOCHEMISTRY AND PETROLOGY, ETH ZÜRICH, CLAUSIUSSTRASSE 25, 8092, SWITZERLAND

[2]MAX PLANCK INSTITUTE FOR CHEMISTRY, 55128, MAINZ, GERMANY

[3]INSTITUTE OF EARTH SCIENCES, UNIVERSITY OF ICELAND, IS-101 REYKJAVIK, ICELAND

RECEIVED FEBRUARY 23, 2010; ACCEPTED OCTOBER 21, 2011
ADVANCE ACCESS PUBLICATION DECEMBER 12, 2011

New trace element and Hf–Nd isotope data on post-glacial basalts from Iceland's main rift zones are used in conjunction with literature data to evaluate the relative importance of source heterogeneity and the melting process for the final melt composition. Correlations between Hf and Nd isotope compositions and trace element ratios indicate that at least two source components are sampled systematically as a function of the degree and pressure of melting beneath Iceland. Strong depletion in Rb, Ba, U and Th and enrichment in Nb and Ta compared with La in the most enriched samples from the Reykjanes Peninsula and Western Rift Zone suggests that the enriched source component is similar to ancient recycled enriched mid-ocean ridge basalt (E-MORB) crust. Highly incompatible trace element ratios such as Nb/La and Nb/U and Pb isotope ratios are variable across Iceland. This observation suggests that either the enriched component is intrinsically heterogeneous, or that there is a larger proportion of the enriched source component beneath the Southwestern Rift Zone compared with the Northern Rift Zone. The relative effect of source heterogeneity and melting on the final melt composition was evaluated with a one-dimensional polybaric melt mixing model in which accumulated melts from a depleted MORB mantle and a recycled E-MORB crust are mixed in different ways. Two styles of melt mixing were simulated: (1) complete mixing of melts with variable proportions of the depleted mantle and recycled E-MORB components; (2) incomplete mixing with a fixed initial proportion of the two source components. Calculated pressure-dependent compositional changes using these simple two-component melting models can explain the observed trends in trace element ratio and isotope ratio diagrams for Icelandic basalts, even in cases where conventional binary mixing models would require more than two source components. The example of Iceland demonstrates that melt mixing during extraction from the mantle is a key process for controlling the trace element and isotope variability observed in basaltic lavas and must be evaluated before inferring the presence of multiple source components.

KEY WORDS: *Iceland; melting; source heterogeneity; trace elements; Hf–Nd isotopes*

INTRODUCTION

Iceland, as part of the Mid-Atlantic Ridge (MAR), is characterized by a geophysical anomaly (gravity, thermal and topography) that has been interpreted to result from buoyant upwelling of hot mantle material (Schilling, 1973; Wolfe, 1997; Shen *et al.*, 1998; Bijwaard & Spakman, 1999; Montelli *et al.*, 2004). Icelandic basalts are compositionally more variable than mid-ocean ridge basalts (MORB) from the adjacent MAR (Jakobsson, 1972; Hart *et al.*, 1973; Schilling, 1973; Elliott *et al.*, 1991; Sigmarsson *et al.*, 1992*b*; Fitton *et al.*, 1997; Blichert-Toft *et al.*, 2005; Kempton *et al.*, 2000; Stracke *et al.*, 2003*c*; Thirlwall *et al.*, 2004; Kokfelt

*Corresponding author. Present address: Department of Petrology, Vrije Universiteit Amsterdam, De Boelelaan 1085, 1081 Hv, The Netherlands. Telephone: +31 20 59 83725. E-mail: janne.koornneef@falw.vu.nl.
†Present address: Institut Für Mineralogie, Westfälische Wilhelms Universität, 48149, Münster, Germany
††Present address: Laboratoire de Géologie de Lyon, Ecole Normale Supérieure de Lyon, UCBL and CNRS, 69364 Lyon Cedex 7, France

et al., 2006). Melt inclusions in Icelandic basalts show even larger variability than their host rocks (Gurenko & Chaussidon, 1995; Slater *et al.*, 2001; Maclennan *et al.*, 2003*a*, 2003*b*; MacLennan, 2008*a*).

In principle, the origin of the large compositional variability observed in Icelandic basalts and melt inclusions is due to either variations in the fractional melting process (i.e. the pressure and degree of melting) or variability in space and/or time of the mantle processed through the melting region. One school of models attributes the observed trace element and isotope variability primarily to source heterogeneity and invokes bulk mixing between different enriched and depleted mantle source components (e.g. Hanan & Schilling, 1997; Chauvel & Hémond, 2000; Hanan *et al.*, 2000; Stracke *et al.*, 2003*c*; Thirlwall *et al.*, 2004; Kokfelt *et al.*, 2006; Kitagawa *et al.*, 2008; Peate *et al.*, 2009). On the basis of the Pb isotope variations observed in Tertiary basalts, Hanan & Schilling (1997) and Hanan *et al.* (2000), for example, suggested the presence of three source components: a depleted N-MORB component 'd', and two enriched components. One enriched component 'e' is similar to EM-1 (Zindler & Hart, 1986); the other enriched plume component 'p' is similar to the common 'C' or 'FOZO' component (Hart *et al.*, 1992; Hanan & Graham, 1996; Stracke *et al.*, 2005). Thirlwall *et al.* (2004) advocated the presence of four major source components based on combined Sr–Nd–Pb isotope data. These major end-members (ID1, ID2, IE1, IE2) were thought to mix at mantle depths to generate intermediate end-member compositions resulting in the near-binary mixing relations observed in the erupted lavas. It has been proposed that isotopic heterogeneity is caused by sampling different components from a recycled oceanic slab: the altered upper basaltic crust, recycled lower gabbroic crust and residual harzburgitic mantle (Chauvel & Hémond, 2000) or recycled oceanic basalts and gabbros with sediments (Kokfelt *et al.*, 2006). Recently, Peate *et al.* (2010) proposed the presence of at least four mantle components based on two separate sub-parallel linear trends on a plot of $^{206}Pb/^{204}Pb$ vs $^{208}Pb/^{204}Pb$ for post-glacial lavas from the Northern and Eastern Volcanic Zones.

Correlations between trace element and isotope compositions in Icelandic basalts, however, indicate that the melting process and sampling of source heterogeneity are intrinsically related. The erupted melts are suggested to represent incomplete mixtures of partial melts from a heterogeneous source, which are extracted from, and integrate over different depths in the melting region (Wood, 1981; Elliott *et al.*, 1991; Maclennan *et al.*, 2003*a*, 2003*b*; Stracke *et al.*, 2003*c*; Kokfelt *et al.*, 2006). In addition to bulk mixing of mantle sources, therefore, mixing of melts from different source components during partial melting appears to play a fundamental role in determining how source heterogeneity is transferred from the source to the melt (Phipps Morgan, 1999; Ito & Mahoney, 2005; Stracke & Bourdon, 2009).

Mixing of melts during partial melting and melt extraction from variable depths has the effect that the isotopic compositions of erupted lavas can differ significantly from those of their bulk mantle source. This observation is in stark contrast to mechanical bulk mixing models, which inherently assume that source heterogeneity is fully conveyed from source to melt. Phipps Morgan (1999) and Ito & Mahoney (2005), for example, demonstrated that progressive melting and mixing of a heterogeneous source can account for the elongated arrays in isotope space for ocean island basalt (OIB) and MORB data. For the specific case of Iceland, the correlations observed between trace elements and isotopes suggest that different source components are tapped systematically as a function of the degree and pressure of melting. Stracke *et al.* (1999, 2003*a*, 2006) and Stracke & Bourdon (2009) showed that factors such as the different solidus temperatures for each of the source components, and the extent, style and depth range of melt aggregation and melt extraction all have important effects on the relationships between trace element and isotope ratios in Icelandic basalts, and MORB and OIB in general.

In this study, we evaluate the relative importance of source heterogeneity, variable degrees of partial melting and melt mixing processes on the final chemical composition of the erupted Icelandic basalts. We focus on post-glacial main-rift lavas, with most samples being younger than 3000 years, to minimize complications by temporal changes in both the melting style and the composition of the mantle entering the melting region (Jull & McKenzie, 1996; Gee *et al.*, 1998*a*; Kempton *et al.*, 2000; Slater *et al.*, 2001; Maclennan *et al.*, 2002; Kitagawa *et al.*, 2008). Our new trace element and Hf and Nd isotope data for young Icelandic rift zone basalts are used in conjunction with existing data on young main-rift lavas to improve sample coverage and spatial resolution. We demonstrate that polybaric melting and variable mixing of melts from only two source components during partial melting and melt extraction can account for the majority of the combined trace element and Nd–Hf–Sr–Pb isotope systematics of Icelandic basalts, even in cases where conventional bulk mixing models would require more than two source components. The example of Iceland thus demonstrates that melt mixing during extraction from the mantle is a key process for controlling the trace element and isotope variability in erupted lavas. Therefore, a better understanding of the partial melting processes and the mechanisms of melt mixing during extraction and subsequent melt evolution is crucial for accurately inferring mantle heterogeneity from MORB and OIB compositions.

GEOLOGY AND SAMPLE COLLECTION

At Iceland, the Mid-Atlantic Ridge emerges in four 40–50 km wide rift zones defined by en-echelon fissure swarms and large central volcanoes. The submarine Reykjanes Ridge in the SW progresses into the subaerial Reykjanes Rift Zone (RRZ) and the Western Rift Zone (WRZ, Fig. 1). The Eastern Rift Zone (ERZ) is connected to the Western Rift Zone via the Southwestern Fracture Zone and continues northwards of the Vatnajökull Icecap as the Northern Rift Zone (NRZ). In the north, the NRZ connects to the submarine Kolbeinsey Ridge via the Tjörnes Fracture Zone. Off-rift volcanic activity occurs in several localities; for example, the Snæfellsnes Peninsula and the Eastern and Southern flank zones. Crustal thickness varies from about 40 km in the centre of Iceland (underneath the Vatnajökull Icecap) to *c.* 15 km under the southwestern part of the Reykjanes Peninsula and 18 km in the NE underneath the Theistareykir area (Allen *et al.*, 2002; Kaban *et al.*, 2002).

Fifty-one post-glacial basalts from Iceland's rift and off-rift zones, which are generally less than 3000 years old, have been collected for this study (Fig. 1, Table 1).

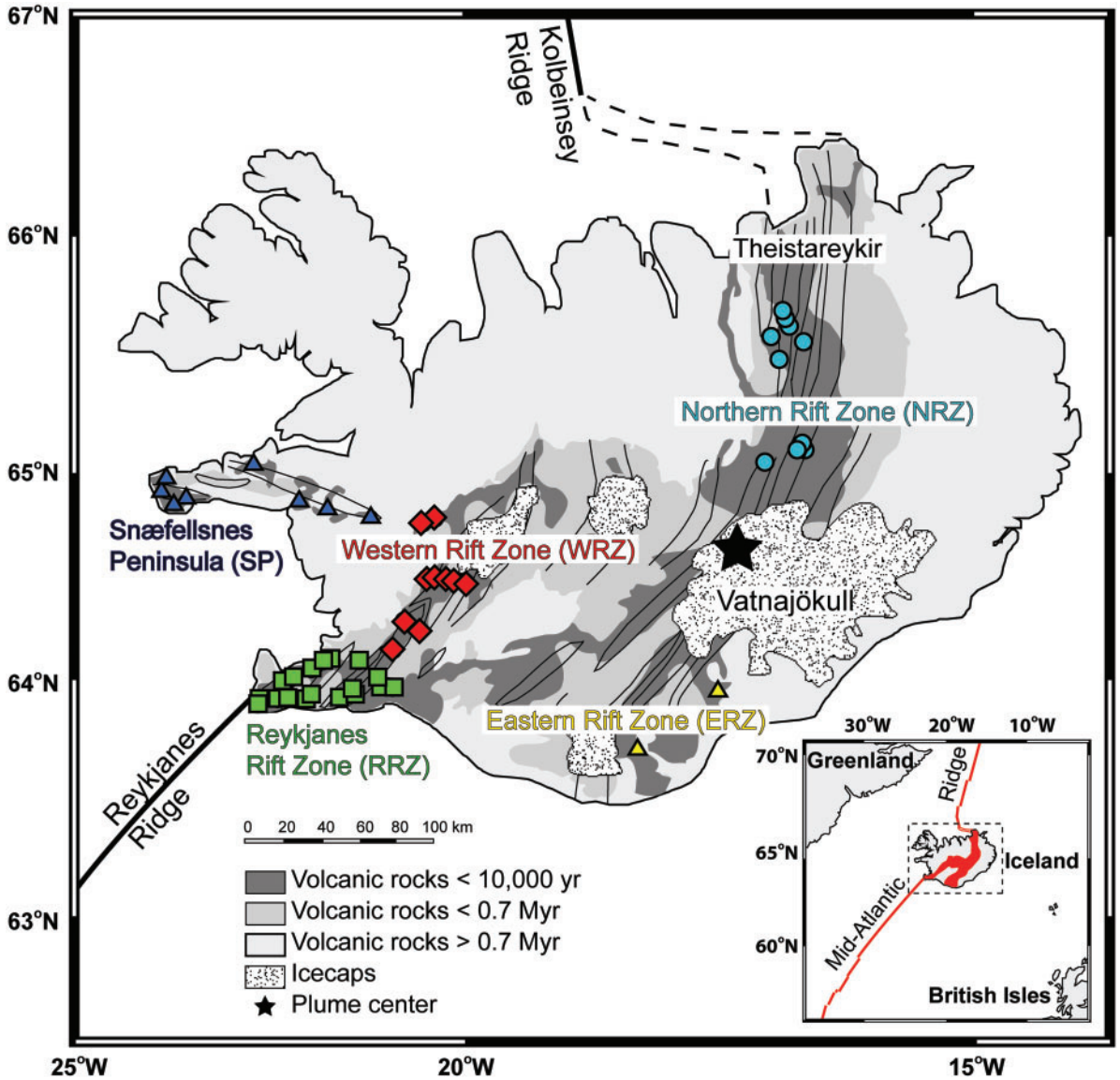

Fig. 1. Simplified geological map of Iceland showing the sampling localities of the 51 lavas investigated here (modified after geological map published at www.¥tephrabase.¥org). Squares, Reykjanes Peninsula (RP); diamonds, Western Volcanics (WV); circles, Northern Volcanics (NV); dark shaded triangles, Snæfellsnes Peninsula (SP); light shaded triangles, Eastern Volcanics (EV). All samples are younger than 10 ka.

Table 1: Major and trace element, and Hf–Nd isotope compositions of Icelandic post-glacial lavas

Sample:	RP1	RP2	RP 3	RP5	RP6	RP7	RP8
Flow name:	Illahraun	Afstapar-Hraun	Arnarseturs-hraun	Stampar-hraun	Eldvarpa-hraun	Eldvarpa-hraun	Arnarseturs-hraun
Age:*	AD 1211–1240	AD 1325	AD 1211–1240	AD 1211–1240	AD 1211–1240	AD 1211–1240	AD 1211–1240
Longitude:	21·991	22·173	22·425	22·709	22·600	22·558	22·420
Latitude:	64·054	64·016	63·928	63·830	63·822	63·819	63·909
Distance from plume (km):	226·4	236·1	254·0	268·0	263·5	261·7	251·6
Major elements (wt %)							
SiO_2	47·84	48·87	48·74	49·22	47·77	48·28	48·57
TiO_2	1·72	1·35	1·82	1·52	1·64	1·93	2·01
Al_2O_3	15·02	13·99	13·50	14·18	14·44	13·89	13·52
Fe_2O_3	12·74	13·24	14·73	13·30	13·49	14·49	14·64
FeO	10·31	10·72	11·93	10·77	10·92	11·73	11·85
MgO	7·93	7·45	6·80	7·26	8·43	7·52	6·76
MnO	0·19	0·21	0·22	0·21	0·20	0·22	0·22
CaO	12·14	12·21	11·33	11·93	11·70	11·37	11·34
Na_2O	2·18	2·24	2·38	2·20	2·18	2·30	2·40
K_2O	0·20	0·18	0·22	0·16	0·16	0·19	0·21
P_2O_5	0·17	0·13	0·20	0·15	0·19	0·20	0·20
Cr_2O_3	0·05	0·02	0·02	0·03	0·05	0·04	0·03
NiO	0·02	0·01	0·01	0·01	0·02	0·01	0·01
Trace elements (ppm)							
V	327	379	451	391	357	409	444
Co	53·6	52·3	55·1	52·8	56·8	55·2	54·9
Ni	119·2	82·8	91·6	92·5	155·7	116·8	88·3
Cu	149	158	172	161	149	161	181
Rb	3·87	3·39	4·11	2·83	2·72	3·34	3·98
Sr	205	156	172	141	188	172	168
Y	25·6	24·1	32·8	26·3	28·0	32·7	31·2
Zr	97·5	71·5	113·8	79·3	103·1	114·7	109·3
Nb	11·3	8·3	12·6	8·3	11·4	12·3	12·3
Cs	0·04	0·04	0·04	0·03	0·03	0·04	0·04
Ba	61·3	53·1	63·7	43·6	48·6	56·1	62·3
La	8·28	6·20	9·01	6·01	7·76	8·59	8·76
Ce	19·3	15·1	21·7	15·1	19·0	21·0	21·5
Pr	2·75	2·15	3·11	2·18	2·75	3·03	3·06
Nd	13·2	10·4	15·1	10·6	13·4	14·8	14·7
Sm	3·53	2·97	4·21	3·08	3·74	4·20	4·07
Eu	1·29	1·12	1·50	1·14	1·35	1·48	1·45
Gd	4·28	3·72	5·19	3·92	4·58	5·25	5·01
Tb	0·70	0·63	0·87	0·66	0·75	0·87	0·84
Dy	4·52	4·24	5·76	4·48	4·89	5·75	5·50
Ho	0·93	0·89	1·20	0·94	1·01	1·19	1·13
Er	2·69	2·61	3·51	2·77	2·91	3·50	3·30
Tm	0·38	0·37	0·50	0·40	0·41	0·49	0·47
Yb	2·53	2·55	3·36	2·74	2·73	3·32	3·18
Lu	0·37	0·38	0·49	0·41	0·41	0·49	0·47
Hf	2·46	1·92	2·92	2·06	2·63	2·98	2·82
Ta	0·72	0·51	0·79	0·51	0·71	0·77	0·75
Pb	0·43	0·31	0·53	0·46	0·48	0·50	0·54
Th	0·57	0·45	0·59	0·41	0·43	0·52	0·56
U	0·16	0·13	0·17	0·12	0·13	0·15	0·17
Hf–Nd isotope composition							
$^{176}Hf/^{177}Hf$	0·283167	0·283199		0·283197	0·283175	0·283186	0·283189
$^{143}Nd/^{144}Nd$	0·513036	0·513057		0·513051	0·513033	0·513051	0·513050

(continued)

Table 1: Continued

Sample:	RP9	RP10	RP11	RP12	RP 13	RP15	RP17
Flow name:	Arnarseturs-hraun	Ögmundar-hraun	Herdísar-vik	Grindas-körð	Hlíðar-vatn	Nesja-hraun	Hólms-hraun
Age:*	AD 1211–1240	AD 1151–1188				~1800 BP	
Longitude:	22·426	22·233	21·786	21·741	21·740	21·445	21·701
Latitude:	63·890	63·854	63·870	63·876	63·875	63·956	64·081
Distance from plume (km):	252·7	245·6	224·9	222·6	226·5	205·8	212·1
Major elements (wt %)							
SiO_2	48·46	48·84	47·84	47·91	47·88	48·28	47·78
TiO_2	1·78	1·46	1·34	1·63	1·67	1·48	1·69
Al_2O_3	13·52	13·94	15·15	14·81	15·12	14·25	15·04
Fe_2O_3	14·60	13·31	11·92	12·94	13·21	13·21	12·74
FeO	11·82	10·78	9·65	10·48	10·70	10·70	10·32
MgO	6·77	7·46	8·22	7·87	7·66	7·68	7·67
MnO	0·22	0·21	0·18	0·20	0·20	0·20	0·19
CaO	11·31	12·23	12·43	12·07	11·99	12·20	12·18
Na_2O	2·37	2·25	2·06	2·23	2·25	2·30	2·24
K_2O	0·21	0·18	0·15	0·20	0·22	0·19	0·18
P_2O_5	0·20	0·13	0·13	0·17	0·18	0·15	0·16
Cr_2O_3	0·02	0·02	0·05	0·04	0·04	0·02	0·04
NiO	0·01	0·01	0·02	0·02	0·02	0·01	0·01
Trace elements (ppm)							
V	428	385	331	354	364	357	368
Co	52·3	53·1	51·8	53·0	53·1	52·4	50·8
Ni	80·7	85·9	159·1	118·2	121·2	90·1	108·2
Cu	187	176	148	167	153	177	161
Rb	4·09	3·52	2·77	3·90	4·23	3·55	3·31
Sr	173	159	181	208	212	202	193
Y	33·3	26·2	22·2	24·9	25·7	25·0	24·7
Zr	116·6	77·2	72·9	93·7	100·6	85·6	85·9
Nb	12·5	8·5	8·6	11·3	12·7	9·2	10·0
Cs	0·05	0·04	0·03	0·04	0·05	0·04	0·03
Ba	63·5	54·2	47·5	62·3	69·4	55·3	53·6
La	9·00	6·52	6·16	8·09	9·00	7·06	7·07
Ce	21·5	15·6	15·2	19·3	21·2	16·9	16·9
Pr	3·08	2·23	2·15	2·71	2·97	2·42	2·43
Nd	15·0	10·9	10·5	13·0	14·0	11·7	11·8
Sm	4·20	3·13	2·92	3·53	3·74	3·28	3·30
Eu	1·48	1·17	1·11	1·29	1·34	1·19	1·22
Gd	5·27	4·00	3·61	4·27	4·44	4·08	3·97
Tb	0·88	0·68	0·60	0·70	0·72	0·68	0·66
Dy	5·80	4·56	3·95	4·48	4·61	4·42	4·32
Ho	1·21	0·96	0·82	0·92	0·94	0·92	0·88
Er	3·56	2·82	2·39	2·66	2·74	2·67	2·54
Tm	0·51	0·40	0·34	0·37	0·38	0·38	0·36
Yb	3·34	2·72	2·21	2·46	2·53	2·51	2·41
Lu	0·50	0·41	0·33	0·36	0·37	0·37	0·36
Hf	3·01	2·06	1·94	2·42	2·56	2·25	2·20
Ta	0·79	0·53	0·52	0·70	0·79	0·58	0·62
Pb	0·57	0·51	0·41	0·54	0·54	0·48	0·47
Th	0·60	0·48	0·40	0·56	0·62	0·50	0·47
U	0·17	0·14	0·12	0·17	0·18	0·14	0·14
Hf–Nd isotope composition							
$^{176}Hf/^{177}Hf$	0·283195	0·283195	0·283180	0·283169		0·283198	0·283170
$^{143}Nd/^{144}Nd$	0·513050	0·513032	0·513044	0·513017		0·513043	0·513042

(continued)

Table 1: Continued

Sample:	RP55	RP56	WV16	WV18	WV19	WV20	WV21
Flow name:	Straums-vik	Ögmundar-hraun	Svínahrauns-bruni	Skjald-breiður I	Skjald-breiður II	Skjald-breiður II	Sköflun-gur
Age:*		AD 1151–1188	~AD 1000				5300 BP
Longitude:	22·027	22·155	21·452	20·920	20·866	20·783	20·650
Latitude:	64·043	63·859	64·028	64·437	64·439	64·444	64·447
Distance from plume (km):	229·0	241·9	202·9	165·3	162·7	158·7	152·3
Major elements (wt %)							
SiO_2	48·83	48·87	47·41	47·68	48·29	48·20	47·54
TiO_2	1·39	1·37	1·59	1·21	1·32	1·30	1·67
Al_2O_3	13·88	14·01	14·42	16·02	14·83	15·64	14·97
Fe_2O_3	13·50	13·28	12·94	11·37	11·59	11·28	12·73
FeO	10·94	10·75	10·48	9·21	9·39	9·14	10·31
MgO	7·46	7·56	9·25	8·99	8·22	7·36	8·47
MnO	0·21	0·21	0·20	0·17	0·18	0·18	0·19
CaO	12·23	12·23	11·54	12·53	12·99	13·12	12·07
Na_2O	2·26	2·21	2·15	1·99	2·01	2·06	2·11
K_2O	0·18	0·17	0·21	0·10	0·14	0·17	0·16
P_2O_5	0·14	0·14	0·17	0·13	0·12	0·13	0·16
Cr_2O_3	0·02	0·02	0·06	0·06	0·05	0·04	0·05
NiO	0·01	0·01	0·02	0·02	0·01	0·01	0·02
Trace elements (ppm)							
V	388	381	338	287	333	323	336
Co	53·0	54·6	56·4	56·7	50·0	48·3	53·7
Ni	84·2	94·7	188·2	191·8	112·4	90·3	143·9
Cu	168·0	192·7	140·3	144·0	157·2	144·8	159·0
Rb	3·45	3·27	3·94	1·33	2·59	3·25	2·62
Sr	167	160	204	169	174	199	195
Y	27·2	24·8	24·6	21·3	21·7	22·4	23·4
Zr	82·4	75·9	95·2	78·0	71·5	79·8	86·0
Nb	9·06	8·61	11·28	7·52	7·32	8·52	9·70
Cs	0·04	0·04	0·04	0·01	0·03	0·04	0·03
Ba	54·1	51·0	62·4	29·6	41·6	51·0	46·0
La	6·77	6·36	8·21	5·41	5·57	6·72	6·79
Ce	16·3	15·5	19·3	13·9	13·6	15·8	16·8
Pr	2·33	2·22	2·72	2·03	1·97	2·23	2·45
Nd	11·4	10·8	13·0	9·9	9·6	10·7	11·9
Sm	3·24	3·08	3·51	2·76	2·77	2·92	3·30
Eu	1·20	1·14	1·26	1·03	1·03	1·07	1·24
Gd	4·15	3·83	4·25	3·43	3·48	3·62	3·98
Tb	0·70	0·65	0·68	0·57	0·58	0·60	0·64
Dy	4·72	4·33	4·44	3·74	3·82	3·93	4·21
Ho	0·99	0·90	0·90	0·77	0·80	0·81	0·86
Er	2·89	2·64	2·61	2·23	2·30	2·38	2·46
Tm	0·41	0·37	0·37	0·31	0·32	0·33	0·34
Yb	2·71	2·59	2·41	2·12	2·21	2·22	2·30
Lu	0·40	0·38	0·35	0·31	0·32	0·33	0·34
Hf	2·16	2·01	2·45	1·87	1·86	2·04	2·18
Ta	0·55	0·53	0·71	0·44	0·46	0·54	0·60
Pb	0·51	0·47	0·38	0·34	0·40	0·48	0·43
Th	0·46	0·45	0·59	0·22	0·38	0·50	0·40
U	0·14	0·13	0·16	0·07	0·11	0·14	0·12
Hf–Nd isotope composition							
$^{176}Hf/^{177}Hf$		0·283218	0·283163	0·283199	0·283204	0·283188	0·283199
$^{143}Nd/^{144}Nd$		0·513036	0·513033	0·513062	0·513068	0·513037	0·513050

(continued)

Table 1: Continued

Sample:	WV21B	WV22	WV25	WV26	WV27	WV30	WV31
Flow name:	Sköflun-gur	Skjald-breiður II	Thjófa-hraun	Thingvalla-hraun	Nesja-hraun	Hallmundar-hraun	Hallmundar-hraun
Age:*	5300 BP		3360 BP	10 200 BP	~1800 BP	AD 1050	AD 1050
Longitude:	20·650	20·694	21·051	21·028	21·247	20·924	20·842
Latitude:	64·447	64·446	64·263	64·145	64·124	64·728	64·745
Distance from plume (km):	159·5	154·4	175·9	179·0	189·8	140·0	158·9
Major elements (wt %)							
SiO_2	47·78	48·31	47·52	47·51	48·04	48·32	48·21
TiO_2	1·91	1·31	1·80	1·36	1·48	1·06	1·00
Al_2O_3	14·79	15·36	14·23	15·08	14·27	15·80	16·00
Fe_2O_3	13·39	11·32	13·50	12·27	13·05	11·29	11·11
FeO	10·84	9·16	10·93	9·94	10·57	9·14	8·99
MgO	7·63	7·74	8·36	8·70	7·67	9·03	9·33
MnO	0·20	0·18	0·20	0·19	0·20	0·18	0·18
CaO	12·09	13·11	11·40	12·53	12·17	12·21	12·10
Na_2O	2·17	2·05	2·20	2·03	2·30	2·14	2·07
K_2O	0·17	0·18	0·21	0·11	0·18	0·11	0·11
P_2O_5	0·19	0·13	0·19	0·17	0·14	0·11	0·10
Cr_2O_3	0·04	0·05	0·05	0·05	0·02	0·02	0·02
NiO	0·01	0·01	0·02	0·02	0·01	0·02	0·02
Trace elements (ppm)							
V	382	318	355	303	365	275	382
Co	53·6	49·1	56·9	53·9	55·9	55·3	53·6
Ni	117	106	159	154	99	169	117
Cu	183	151	163	143	167	148	183
Rb	3·10	3·43	3·98	1·65	3·41	2·18	3·10
Sr	192	198	200	186	198	139	192
Y	27·7	21·6	26·9	23·1	24·0	22·2	27·7
Zr	102	79	111	83	82	60	102
Nb	11·3	8·7	12·6	10·7	9·0	5·2	11·3
Cs	0·03	0·03	0·04	0·02	0·04	0·02	0·03
Ba	51·3	51·4	60·7	36·0	54·4	30·7	51·3
La	7·9	6·8	9·4	6·7	6·9	4·2	7·9
Ce	19·4	16·2	22·5	16·7	16·8	10·1	19·4
Pr	2·82	2·28	3·16	2·45	2·42	1·52	2·82
Nd	13·8	10·8	14·9	11·8	11·7	7·7	13·8
Sm	3·84	2·92	3·96	3·23	3·23	2·40	3·84
Eu	1·40	1·06	1·41	1·17	1·20	0·91	1·40
Gd	4·63	3·52	4·62	3·83	3·97	3·22	4·63
Tb	0·76	0·58	0·75	0·63	0·66	0·56	0·76
Dy	4·92	3·75	4·81	4·14	4·34	3·81	4·92
Ho	1·01	0·77	0·98	0·85	0·90	0·81	1·01
Er	2·90	2·23	2·79	2·44	2·62	2·43	2·90
Tm	0·41	0·32	0·39	0·34	0·37	0·34	0·41
Yb	2·74	2·16	2·66	2·31	2·45	2·31	2·74
Lu	0·40	0·31	0·39	0·34	0·36	0·34	0·40
Hf	2·61	1·99	2·75	2·03	2·18	1·64	2·61
Ta	0·71	0·53	0·77	0·64	0·58	0·33	0·71
Pb	0·53	0·41	0·62	0·34	0·46	0·29	0·53
Th	0·47	0·49	0·62	0·25	0·48	0·34	0·47
U	0·14	0·15	0·19	0·07	0·14	0·09	0·14
Hf–Nd isotope composition							
$^{176}Hf/^{177}Hf$		0·283173	0·283164	0·283191	0·283184		0·283224
$^{143}Nd/^{144}Nd$		0·513055	0·513034	0·513051	0·513041		0·513069

(continued)

Table 1: Continued

Sample:	SP 28	SP29	SP 32 A	SP 32 B	SP 33	SP 34	SP 35
Flow name:	Gábrókar-hraun	Bifrost, Gábró-karhraun	Rauðhálsa-hraun	Rauðhálsa-hraun	Miðhraun	Porserkja-hraun	Porserkja-hraun
Age:*			historical	historical	<4000 BP	<4000 BP	<4000 BP
Longitude:	21·578	21·578	22·291	22·291	22·661	22·931	22·946
Latitude:	64·747	64·747	64·834	64·834	64·860	64·973	64·971
Distance from plume (km):	203·0	193·8	237·0	237·0	259·0	268·0	271·5
Major elements (wt %)							
SiO_2	47·35	47·14	47·47	47·50	46·67	46·53	47·07
TiO_2	1·61	1·50	1·52	1·60	1·47	1·45	1·94
Al_2O_3	15·20	15·16	14·65	14·63	13·83	12·07	13·64
Fe_2O_3	12·05	11·90	11·88	11·86	11·13	11·05	10·81
FeO	9·76	9·64	9·62	9·61	9·02	8·95	8·76
MgO	9·32	9·30	9·43	9·60	11·81	14·54	10·88
MnO	0·19	0·19	0·19	0·19	0·18	0·18	0·18
CaO	11·67	11·59	11·65	11·69	12·14	11·36	11·67
Na_2O	2·23	2·19	2·23	2·24	2·09	1·78	2·18
K_2O	0·49	0·48	0·56	0·56	0·27	0·55	0·84
P_2O_5	0·19	0·19	0·21	0·21	0·18	0·22	0·31
Cr_2O_3	0·04	0·04	0·07	0·07	0·13	0·24	0·13
NiO	0·02	0·02	0·02	0·02	0·04	0·05	0·03
Trace elements (ppm)							
V	235	229	317	305	291	280	294
Co	40·6	40·1	56·3	55·4	58·9	64·2	51·4
Ni	105	107	190	185	284	417	220
Cu	74·3	73·1	110·2	110·0	72·0	87·7	79·8
Rb	7·75	7·52	13·19	13·44	6·28	12·96	19·61
Sr	205	199	264	272	207	301	408
Y	14·6	15·1	23·7	21·4	23·3	19·3	21·2
Zr	74·7	77·2	125·0	115·8	82·4	114·8	163·9
Nb	13·6	13·1	23·0	22·8	11·6	24·6	38·4
Cs	0·09	0·09	0·14	0·16	0·07	0·13	0·19
Ba	101	96	159	163	86	184	283
La	10·5	10·2	17·0	16·5	9·1	17·5	27·4
Ce	23·2	22·0	36·8	36·4	20·9	35·8	56·5
Pr	3·02	2·87	4·65	4·56	2·88	4·49	6·79
Nd	13·0	12·6	19·9	19·4	13·5	19·3	27·8
Sm	2·89	2·82	4·33	4·21	3·48	4·06	5·46
Eu	0·99	0·93	1·41	1·39	1·22	1·30	1·70
Gd	2·92	2·94	4·55	4·30	4·05	4·08	5·01
Tb	0·44	0·44	0·69	0·65	0·65	0·60	0·71
Dy	2·76	2·76	4·29	4·02	4·21	3·60	4·16
Ho	0·55	0·55	0·86	0·80	0·86	0·71	0·79
Er	1·55	1·56	2·43	2·25	2·46	1·95	2·13
Tm	0·22	0·21	0·34	0·31	0·34	0·27	0·29
Yb	1·42	1·42	2·22	2·10	2·28	1·74	1·92
Lu	0·21	0·21	0·33	0·31	0·34	0·26	0·28
Hf	1·85	1·91	2·99	2·78	2·19	2·79	3·75
Ta	0·84	0·82	1·39	1·36	0·75	1·56	2·35
Pb	0·70	0·65	1·10	1·01	0·57	0·90	0·92
Th	0·99	0·99	1·68	1·62	0·84	1·84	2·97
U	0·29	0·28	0·48	0·49	0·24	0·48	0·84
Hf–Nd isotope composition							
$^{176}Hf/^{177}Hf$		0·283135					
$^{143}Nd/^{144}Nd$		0·512941					

(continued)

Table 1: Continued

Sample:	SP36	NV41	NV42	NV43	NV44	NV45	NV47
Flow name:	Prestahraun	Prengs-laborgir	Elda	Nyarhraun	Búrfells-hraun	Krafla	Krafla
Age:*	<4000 BP	~3000 BP	AD 1729	AD 1875	~3000 BP	AD 1729	AD 1984
Longitude:	23·959	16·948	16·945	16·390	16·752	16·784	16·791
Latitude:	64·881	65·575	65·656	65·651	65·649	65·718	65·716
Distance from plume (km):	306·7	104·2	129·1	130·0	113·0	121·5	141·5
Major elements (wt %)							
SiO_2	45·72	48·94	49·37	50·15	48·80	49·78	49·79
TiO_2	2·47	1·54	2·02	2·78	1·64	2·02	2·09
Al_2O_3	14·38	14·16	13·20	12·64	14·23	13·22	13·07
Fe_2O_3	12·28	12·53	16·08	17·17	13·32	16·21	16·40
FeO	9·94	10·15	13·02	13·90	10·78	13·12	13·28
MgO	9·92	7·75	5·88	4·75	7·66	5·94	5·82
MnO	0·19	0·20	0·24	0·26	0·21	0·24	0·24
CaO	11·65	12·66	10·24	9·11	12·11	10·22	10·27
Na_2O	2·32	2·20	2·50	2·95	2·22	2·47	2·51
K_2O	0·72	0·16	0·32	0·52	0·20	0·32	0·32
P_2O_5	0·50	0·14	0·21	0·31	0·16	0·21	0·21
Cr_2O_3	0·08	0·02	0·02	0·01	0·02	0·02	0·02
NiO	0·02	0·01	0·01	0·01	0·01	0·01	0·01
Trace elements (ppm)							
V	336	342	476	528	336	481	493
Co	50·5	53·0	54·9	49·8	50·8	53·3	53·6
Ni	174·0	90·9	74·4	38·5	88·9	66·1	62·5
Cu	59·7	168·8	153·4	125·4	168·6	151·1	160·5
Rb	14·52	3·17	7·12	11·26	3·77	6·90	7·25
Sr	447	162	160	197	186	164	165
Y	24·7	26·3	38·2	41·3	23·8	38·2	36·5
Zr	171·0	89·2	129·7	170·0	85·3	128·1	125·3
Nb	37·1	7·7	11·3	19·8	9·1	11·1	11·9
Cs	0·1	0·0	0·1	0·1	0·0	0·1	0·1
Ba	355·8	36·4	86·6	117·2	51·2	85·2	88·8
La	26·1	6·2	9·7	15·2	6·7	9·5	9·8
Ce	54·9	15·5	23·0	36·5	16·9	22·6	24·2
Pr	7·01	2·26	3·28	5·02	2·45	3·22	3·41
Nd	30·1	11·3	16·0	23·2	11·8	15·7	16·4
Sm	6·02	3·27	4·55	6·10	3·32	4·45	4·60
Eu	2·14	1·19	1·56	2·06	1·24	1·55	1·63
Gd	5·73	4·18	5·81	7·14	4·07	5·79	5·72
Tb	0·81	0·70	0·98	1·17	0·68	0·98	0·97
Dy	4·72	4·66	6·57	7·49	4·36	6·58	6·43
Ho	0·91	0·96	1·38	1·52	0·89	1·39	1·35
Er	2·49	2·76	4·06	4·47	2·60	4·09	3·96
Tm	0·33	0·39	0·59	0·62	0·36	0·59	0·57
Yb	2·16	2·61	3·99	4·20	2·47	3·95	3·87
Lu	0·32	0·38	0·60	0·61	0·36	0·60	0·57
Hf	3·73	2·33	3·32	4·32	2·26	3·33	3·24
Ta	2·26	0·50	0·72	1·23	0·57	0·71	0·73
Pb	0·93	0·46	0·77	1·11	0·41	0·80	0·85
Th	1·79	0·51	0·79	1·37	0·45	0·81	0·80
U	0·48	0·15	0·22	0·39	0·13	0·22	0·24
Hf–Nd isotope composition							
$^{176}Hf/^{177}Hf$	0·283128	0·283204	0·283201		0·283192	0·283198	
$^{143}Nd/^{144}Nd$	0·512960	0·513078	0·513040		0·513048	0·513034	

(continued)

Table 1: Continued

Sample:	NV48	NV49	NV50	NV51	NV52	NV53	NV54
Flow name:	Daleldar		Krafla	Askja	Askja	Askja	Frambruni
Age:*	3000 BP	AD 1984	AD 1984	AD 1961	~AD 1920	AD 1961	>AD 1362
Longitude:	16·793	16·841	16·841	16·638	16·721	16·770	17·075
Latitude:	65·664	65·795	65·795	65·057	65·044	64·914	65·017
Distance from plume (km):	115·7	129·1	114·6	67·5	55·7	44·2	43·8
Major elements (wt %)							
SiO_2	49·60	49·04	49·20	50·15	50·03	50·43	49·74
TiO_2	2·05	1·60	1·60	2·80	2·77	2·76	1·41
Al_2O_3	12·91	14·19	14·21	12·64	12·63	12·74	14·49
Fe_2O_3	16·70	14·01	14·04	16·97	16·90	16·94	12·68
FeO	13·52	11·34	11·37	13·74	13·68	13·72	10·27
MgO	5·62	7·32	7·34	4·71	4·73	4·80	6·77
MnO	0·25	0·21	0·21	0·25	0·25	0·25	0·20
CaO	10·00	11·38	11·40	9·06	9·12	9·25	12·14
Na_2O	2·49	2·22	2·22	2·93	2·91	2·88	2·37
K_2O	0·32	0·24	0·24	0·53	0·52	0·52	0·21
P_2O_5	0·20	0·17	0·17	0·31	0·31	0·31	0·15
Cr_2O_3	0·01	0·04	0·04	0·00	0·01	0·01	0·02
NiO	0·01	0·01	0·01	0·01	0·00	0·01	0·01
Trace elements (ppm)							
V	472	381	393	533	541	513	349
Co	53·5	50·4	52·7	50·1	50·7	48·5	50·5
Ni	56·0	109·1	116·5	30·5	33·1	36·1	67·5
Cu	157	146	148	124	128	121	145
Rb	7·09	5·15	5·15	12·15	11·63	12·24	4·60
Sr	158	171	173	198	195	204	163
Y	36·4	29·4	27·6	49·6	47·1	45·7	29·1
Zr	118·1	96·6	92·1	214·0	201·4	191·0	104·4
Nb	11·3	9·4	9·8	21·1	20·5	21·2	8·7
Cs	0·08	0·06	0·06	0·13	0·12	0·13	0·04
Ba	85·2	66·2	68·1	123·2	119·5	126·5	44·8
La	9·3	7·5	7·7	17·0	16·2	16·8	7·1
Ce	22·5	18·3	19·2	39·2	38·0	39·8	17·6
Pr	3·19	2·65	2·74	5·41	5·21	5·47	2·53
Nd	15·4	13·0	13·3	25·6	24·5	25·6	12·4
Sm	4·38	3·72	3·74	6·81	6·46	6·84	3·60
Eu	1·52	1·34	1·38	2·19	2·11	2·26	1·28
Gd	5·59	4·69	4·57	8·22	7·82	8·07	4·54
Tb	0·94	0·79	0·77	1·34	1·27	1·32	0·77
Dy	6·32	5·32	5·11	8·73	8·24	8·63	5·10
Ho	1·33	1·11	1·05	1·80	1·70	1·76	1·06
Er	3·96	3·28	3·14	5·19	4·88	5·16	3·08
Tm	0·57	0·46	0·44	0·74	0·69	0·73	0·43
Yb	3·91	3·09	2·98	4·83	4·61	4·72	2·89
Lu	0·59	0·46	0·43	0·72	0·69	0·69	0·42
Hf	3·19	2·66	2·49	5·37	5·05	5·10	2·67
Ta	0·73	0·61	0·61	1·36	1·29	1·39	0·56
Pb	0·79	0·59	0·62	1·31	1·26	1·22	0·54
Th	0·76	0·57	0·56	1·66	1·57	1·60	0·70
U	0·22	0·17	0·17	0·45	0·43	0·45	0·19
Hf–Nd isotope composition							
$^{176}Hf/^{177}Hf$	0·283194	0·283188	0·283191		0·283185	0·283180	0·283197
$^{143}Nd/^{144}Nd$	0·513053	0·513044	0·513029		0·513028	0·513047	0·513032

(continued)

Table 1: Continued

Sample:	EV57	EV58	USGS BHVO
Flow name:	Eldhraun/ skaftafellhraun	Hólmshraun	reference material
Age:*	AD 1783	AD 934	Average ($n=3$)
Longitude:	17·739	18·541	
Latitude:	63·891	63·629	
Distance from plume (km):	72·5	110·0	
Major elements (wt %)			
SiO_2	49·31	45·89	
TiO_2	2·71	4·31	
Al_2O_3	13·61	12·68	
Fe_2O_3	14·50	16·90	
FeO	11·74	13·68	
MgO	5·64	5·50	
MnO	0·21	0·21	
CaO	10·54	10·60	
Na_2O	2·78	2·82	
K_2O	0·40	0·60	
P_2O_5	0·29	0·41	
Cr_2O_3	0·01	0·01	
NiO	0·01	0·01	
Trace elements (ppm)			
V	410	558	329
Co	47·9	56·4	44·9
Ni	46·0	64·2	124
Cu	104	153	132
Rb	7·86	12·26	9·19
Sr	241	404	390
Y	38·6	33·3	27·7
Zr	188	219	188
Nb	17·7	28·8	17·8
Cs	0·07	0·14	0·09
Ba	84·7	151	130
La	13·7	22·2	15·5
Ce	33·4	51·2	37·2
Pr	4·69	6·90	5·24
Nd	22·4	31·6	24·7
Sm	6·07	7·62	6·12
Eu	2·05	2·53	2·03
Gd	7·12	7·84	6·49
Tb	1·13	1·15	0·96
Dy	7·12	6·67	5·57
Ho	1·42	1·23	1·02
Er	3·97	3·22	2·67
Tm	0·55	0·42	0·34
Yb	3·53	2·63	2·13
Lu	0·51	0·36	0·29
Hf	4·64	5·25	4·67
Ta	1·14	1·87	1·15
Pb	0·86	1·47	1·64
Th	1·19	2·11	1·28
U	0·32	0·60	0·40
Hf–Nd isotope composition			
$^{176}Hf/^{177}Hf$			
$^{143}Nd/^{144}Nd$			

*Ages are from Peate *et al.* (2009) and Sinton *et al.* (2005).
Major element compositions were determined by XRF at ETH Zurich. FeO is calculated using Fe^{2+}/Fe^{3+} of 0·9. Trace element concentrations were measured by LA-ICP-MS at the Max Planck Institute for Chemistry, Mainz. Hf and Nd isotope compositions were measured by MC-ICP-MS and Triton thermal ionization mass spectrometry at ETH Zurich.

Sampling focused on collecting fresh and relatively undifferentiated samples to minimize the influence of crustal processes. We distinguish five sample groups: samples from the Reykjanes Peninsula (RP), the Western, Eastern and Northern Volcanics (WV, EV and NV, respectively) and the off-rift basalts from the Snæfellsnes Peninsula (SP, Fig. 1). The majority of the samples ($n=42$) are tholeiitic basalts but also include alkalic basalts from the off-rift Snæfellsnes Peninsula ($n=7$) and the Eastern Volcanic Zone ($n=2$). Tholeiites range from aphyric to porphyritic rocks containing phenocrysts of plagioclase (2–10 mm) and lesser amounts of olivine (0·5–5 mm) and accessory magnetite (<1 mm). Total amounts of phenocrysts typically are below 10%. Only alkali basalts contain a larger amount of olivine (0·5–5 mm), clinopyroxene (0·5–10 mm) and plagioclase (0·5–7 mm), with total phenocryst contents estimated between 5 and 20%.

ANALYTICAL TECHNIQUES

Hand specimens free of weathered surfaces were cut and crushed using a diamond saw, a hydraulic press and an agate mill to produce a homogeneous rock powder. Major elements were analysed by X-ray fluorescence (XRF) at ETH Zürich on glass beads produced using di-lithium tetraborate as a flux agent. Trace elements were analysed by laser ablation inductively coupled plasma mass spectrometry (LA-ICP-MS) at the Max Planck Institute for Chemistry, Mainz using a solid-state 213 nm Nd:YAG laser connected to a Thermo Element 2. The LA-ICP-MS analyses were carried out on glasses produced from 40 mg sample powders using an automated Iridium Strip heater (Stoll *et al.*, 2008). The fused glass beads were analysed nine times (100 μm spots) to account for possible heterogeneities. ^{43}Ca (calculated from CaO wt % obtained by XRF) was used as an internal standard and all analyses were externally calibrated with reference glasses KL-2G and GSD-G, which were interspersed after every third sample. Replicate analyses of BHVO-2 ($n=3$) indicate an external reproducibility of less than 3% (2 SD) for all measured elements except Ni, Rb, Ba, Eu, Ta, U and Th, which reproduced to 3–5%, and Cs, with an external reproducibility of about 8% (2 SD). Pb concentrations cannot be measured precisely (2 SD = 50%) with this technique owing to the volatile behaviour of Pb during the glass fusion process (Stoll *et al.*, 2008). The BHVO-2 concentrations are within 3% of the preferred values (http://georem.mpch-mainz.gwdg.de) for Co, Rb, Sr, Nb, Ba, La, Ce, Pr, Nd, Sm, Eu, Ta and U; between 3 and 6% for V, Ni, Cu, Y, Cs, Gd, Tb, Dy, Ho, Er, Tm and Th; and better than 9% for Zr, Lu, Hf and Yb. The accuracy of the technique for low concentration elements is further confirmed by determinations of U concentrations by isotope dilution. The U concentration data obtained from both techniques generally agree within 10% (see

Supplementary Data I, available for downloading at http://www.petrology.oxfordjournals.org).

For Hf and Nd isotope analyses *c.* 100 mg of sample powder was dissolved in a mixture of HF and HNO_3. After dissolution samples were converted to a chloride form and at this stage boric acid was added to complex any remaining fluorides. Hf was separated from the matrix with Eichrom^{TM} LN-spec resin (100–150 mesh) using the technique described in detail by Münker *et al.* (2001). The fraction from the first Hf column was used for separation of bulk REE on a 0·5 ml TRU-spec column (50–100 mesh). Nd was purified using a 1·5 ml LN spec column (50–100 mesh) adapted from Pin & Zalduegui (1997). Hf isotope analyses were performed by multi-collector (MC)-ICP-MS on a Nu Instruments system at ETH Zürich in static mode using $^{179}Hf/^{177}Hf = 0{\cdot}7325$ as a reference for exponential mass fractionation correction. ^{172}Yb and ^{175}Lu were monitored and used to correct isobaric interferences on ^{176}Hf. The contribution of ^{176}Yb to the ^{176}Hf signal never exceeded 0·012% during analysis and is therefore within the reported analytical error. Repeated measurements of JMC-475 during the analysis period yielded a mean of $^{176}Hf/^{177}Hf = 0{\cdot}282194 \pm 16$ (2 SD, $n = 15$). The measured Hf isotope values were corrected by sample–standard bracketing using JMC-475 $^{176}Hf/^{177}Hf = 0{\cdot}282160$ (Blichert-Toft & Albarède, 1997). Accuracy and precision of the full analytical procedure was monitored by repeated measurements of USGS rock reference material BCR-2 and BHVO-2 over an 8 month period. $^{176}Hf/^{177}Hf$ ratios of $0{\cdot}282861 \pm 25$ (2 SD, $n = 7$) for BCR-2 and $0{\cdot}283107 \pm 16$ (2 SD, $n = 5$) for BHVO-2 are in excellent agreement with reported literature values (Table 1; e.g. Chu *et al.*, 2002; Bizzarro *et al.*, 2003; Weis *et al.*, 2007).

Nd isotopic compositions were determined by thermal ionization mass spectrometry (TIMS) on a Thermo Triton at ETH Zürich. Instrumental mass fractionation was corrected with an exponential law using $^{146}Nd/^{144}Nd = 0{\cdot}7219$. The La Jolla Nd standard yielded an average $^{143}Nd/^{144}Nd$ of $0{\cdot}511855 \pm 15$ ($n = 21$) over the measurement period. Blanks are ~380 pg for Hf and ~225 pg for Nd, and are insignificant compared with the analysed amount of sample.

RESULTS

Major elements

Major and trace element concentrations for the 51 samples are reported in Table 1. The main rift lavas are olivine tholeiites with MgO between 4·7 and 9·3 wt %. The dominant phases in equilibrium with primitive Icelandic rift-zone basalts are olivine, clinopyroxene (cpx) and plagioclase (plag), with chromium spinel and magnetite as accessory phases (Carmichael, 1964; Jakobsson, 1972; Maclennan *et al.*, 2003*a*; Gurenko & Sobolev, 2006). Fractional crystallization of the primitive magmas results in consecutive lowering of the MgO (olivine), CaO (cpx, plag), and Al_2O_3 (plag) contents. Our samples define trends of olivine (ol), plagioclase (plag) and clinopyroxene (cpx) fractionation, with the sample groups (RP, WV, NV, EV and SP) showing differences in both the mineral proportions of the fractionating assemblage and in the absolute degree of crystal fractionation. These data are consistent with previously reported data for Icelandic lavas (Fig. 2).

The Northern and Eastern Volcanics generally have lower MgO contents compared with the Western Volcanics (MgO 4·7–7·8 wt % compared with 7·4–9·3 wt %) and exhibit a positive correlation on diagrams of MgO vs CaO/Al_2O_3 and Al_2O_3/TiO_2 (Fig. 2d and f). This observation indicates higher degrees of fractional crystallization for the NV and EV samples compared with the WV samples, with a greater proportion of plagioclase and clinopyroxene in the fractionating assemblage (CaO/Al_2O_3 and Al_2O_3/TiO_2 decrease with decreasing MgO). The WV samples define a trend of combined olivine and plagioclase fractionation (CaO/Al_2O_3 increases but Al_2O_3/TiO_2 decreases with decreasing MgO) and are not significantly affected by cpx fractionation. Samples from the Reykjanes Peninsula have intermediate MgO (6·8–8·4 wt %), CaO/Al_2O_3 and Al_2O_3/TiO_2 and have similar major element compositions to the least differentiated NV samples. The alkali basalts from the Snæfellsnes Peninsula have the highest MgO contents, ranging from 9·3 to 14·5 wt % MgO, and are dominated by cpx and olivine crystallization at pressures higher than the main rift lavas. Negative correlations on diagrams of MgO vs K_2O, Na_2O and TiO_2, defined by the NV and EV samples, reflect the incompatibility of these elements during the entire fractional crystallization process (Fig. 2a, b and e).

Trace elements

Primitive mantle normalized trace element patterns are shown in Fig. 3, with the samples grouped by geographical area. Overall, the Iceland samples display large to moderate enrichments in light rare earth elements (LREE) and highly incompatible elements (Ba, Rb, U, Th, Nb, Ta; Fig. 3a) relative to primitive mantle (McDonough & Sun, 1995). Compared with neighbouring elements, all lavas are enriched in Ba, Nb and Ta and depleted in Th, U and K. Relative fractionation between Nb, Ta and neighbouring elements such as U, Th and La are largest for samples from the Reykjanes Peninsula and the Western Volcanic Zone (Fig. 3b and c).

The Western Volcanics are the least LREE enriched. Two WV lavas from Hallmundarhraun (WV30 and WV31) have $La_N = 4{\cdot}5$, and relatively flat REE patterns with $(La/Yb)_N = 1{\cdot}2$ and $(La/Sm)_N = 1{\cdot}1$ (Fig. 3c, Table 1; the subscript N denotes primitive mantle normalized values). The majority of the WV samples, however, have La_N varying from 7·5 to 10·5 and $(La/Sm)_N = 1{\cdot}2–1{\cdot}5$. Basalts from

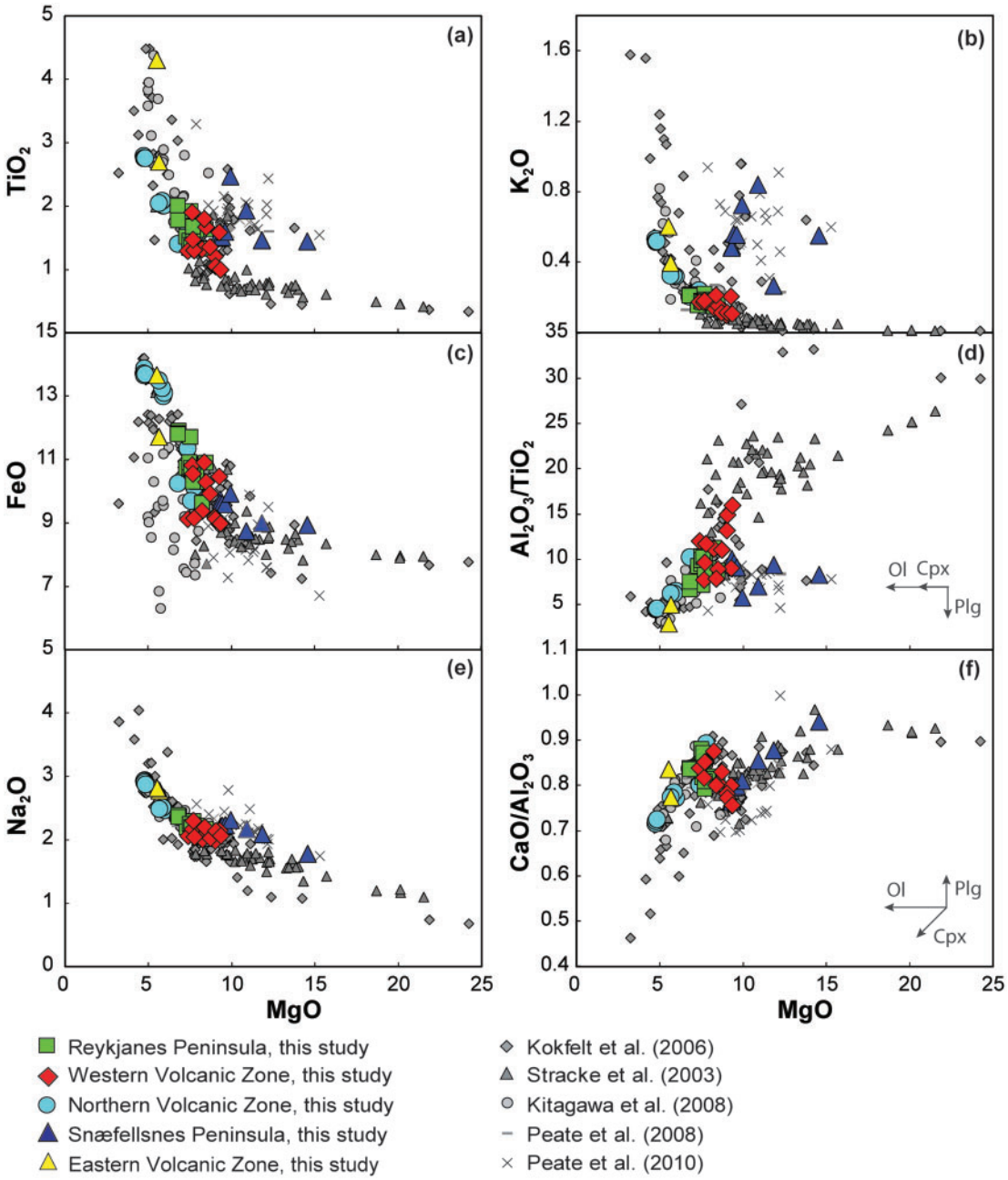

Fig. 2. Variation of whole-rock major element concentrations and ratios in Icelandic basalts from each of the rift zones vs MgO (wt %). Symbols for the data plotted here are as in Fig. 1. Literature data shown are from studies that allow comparison with the trace element and isotope data (see legend for references). Fractional crystallization results in consecutive lowering of the MgO (olivine), CaO (cpx, plag), and Al_2O_3 (plag). The arrows in (d) and (f) indicate the effect. Samples from the different areas show both differences in the mineral proportion of the fractionating assemblage and in the absolute degree of crystal fractionation. WV samples lie on trends of combined olivine and plagioclase fractionation whereas RP and NV samples lie on trends indicative of simultaneous plagioclase and clinopyroxene fractionation. NV samples with low MgO (4·7–6 wt %) are characterized by significant fractionation of clinopyroxene and plagioclase. These more evolved samples are highlighted in Figs 4 and 6 by a cross.

the Reykjanes Peninsula (RP) and the Northern Volcanic Zone (NV) have La_N varying between 9 and 14, similar to those of the WV samples. Samples from Askja volcano, in the Northern Volcanic Zone (NV51–NV53) are exceptional among this group because they are more enriched ($La_N \sim 26$ vs 12) and more fractionated ($La/Yb_N = 2{\cdot}4$ vs 1·9) with pronounced relative depletions in Sr, indicative of a higher relative amount of plagioclase

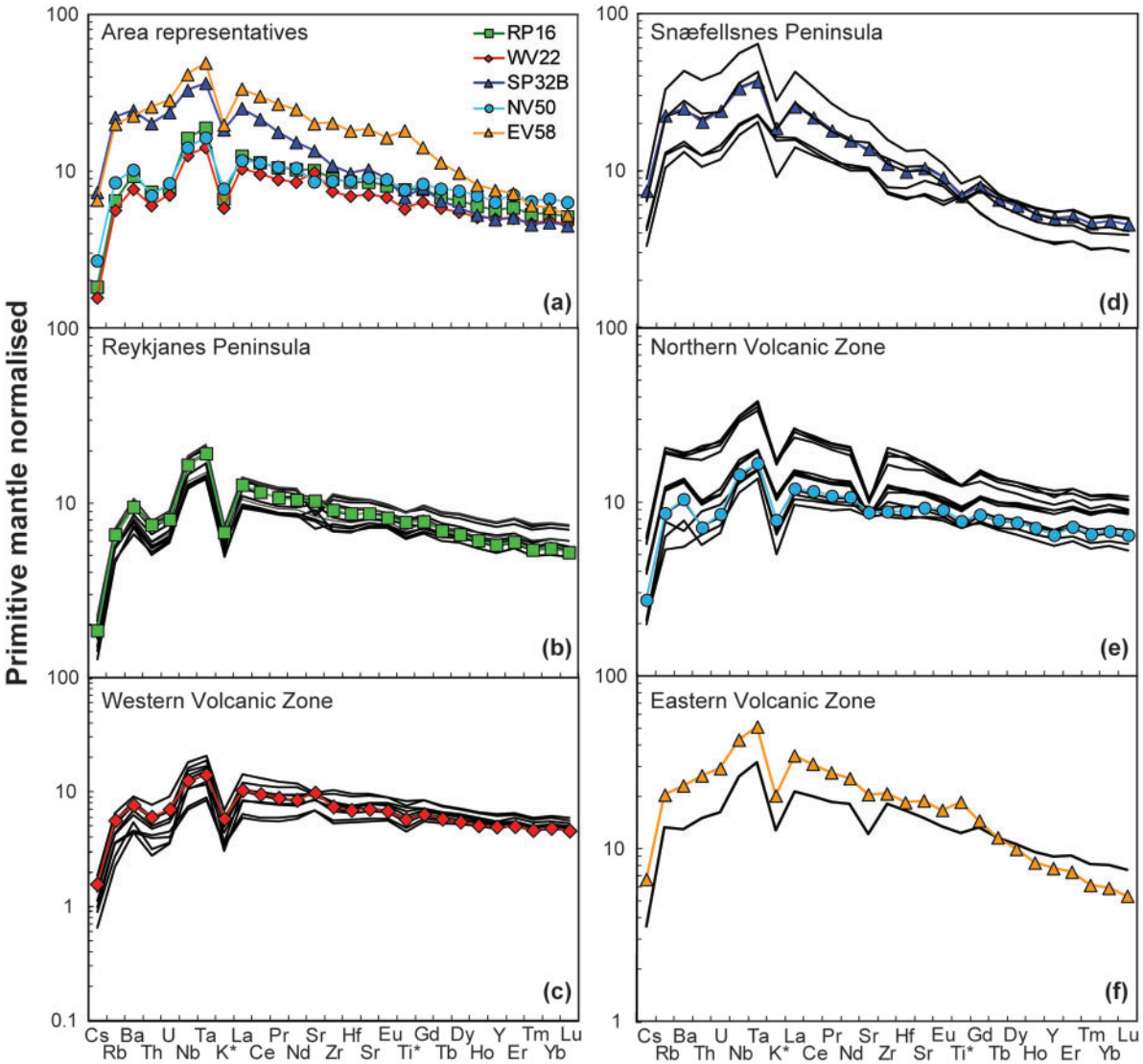

Fig. 3. Primitive mantle normalized multi-element patterns for all samples from each geographical area (b–f). Representative samples from each area (RP16, WV22, SP35, NV50, EV58) are highlighted and are shown in (a) for direct comparison. Primitive mantle values are from McDonough & Sun (1995).

fractionation compared with the other NV samples. Alkali basalt lavas from the Snæfellsnes Peninsula (SP) are highly enriched and fractionated with La_N ranging from 16 to 40 and have fractionated heavy REE (HREE) patterns with $(Sm/Yb)_N$ varying from 1·7 to 3·2 (Fig. 3d). HREE patterns for RP, WV and NV samples, on the other hand, are flat with $(Sm/Yb)_N = 1·3–1·6$.

Incompatible trace element concentrations (e.g. La, Y, U) and ratios (e.g. La/Sm, Sm/Yb, Lu/Hf, Y/Nb) are generally correlated with major element concentrations and ratios (e.g. FeO, K_2O, TiO_2, K_2O/TiO_2, CaO/Na_2O, Al_2O_3/TiO_2; Fig. 4a). Incompatible element contents (e.g. K_2O) or ratios such as La/Yb and La/Sm generally decrease with increasing degree of melting, whereas Fe_2O_3 and Lu/Hf increase and SiO_2/FeO decreases with increasing pressure of melting (Table 1 and Fig. 4a). Because fractional crystallization has a negligible effect on the trace element concentrations (see detailed discussion below), the major and trace element concentrations and ratios reflect progressive melting with decreasing pressure (see also Elliott *et al.*, 1991; Stracke *et al.*, 2003*c*).

Data for the main rift lavas from this study fit into the general correlations observed for Iceland (Fig. 4a; Chauvel & Hémond, 2000; Stracke *et al.*, 2003*c*; Kokfelt *et al.*, 2006; Kitagawa *et al.*, 2008; Peate *et al.*, 2009, 2010). There is no systematic relation between the observed

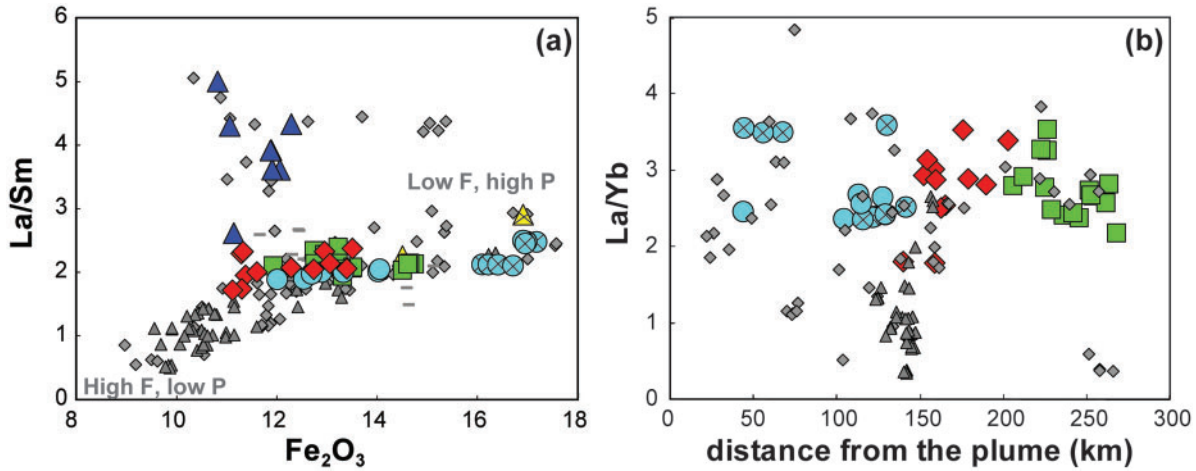

Fig. 4. (a) Variation of La/Sm vs Fe_2O_3 for all Icelandic lavas and (b) La/Yb vs distance to the plume centre associated with the Icelandic main rift lavas. The correlation between Fe_2O_3 and La/Sm for Icelandic lavas observed in (a) indicates a relation between the pressure (*P*) and the degree (*F*) of melting. Fe_2O_3 increases with increasing pressure of melting whereas incompatible element contents and ratios such as La/Sm decrease with increasing degree of melting. (b) shows that the variability of La/Yb in the main rift lavas on a local scale is as large as the overall variability across Iceland, indicating that the melting behaviour along the rift is primarily controlled by the local melting process and not by a large-scale temperature anomaly across the Iceland plume. Samples from off-rift areas are excluded from (b) as these are probably influenced by the presence of a thicker lithospheric lid and are therefore not suitable for comparison. Symbols are as in Fig. 2. Samples with MgO <6 wt % are highlighted with a cross.

variations and the geographical areas (i.e. RP, WV, NV), and thus distance to the plume centre (Fig. 4b). Overall, the basalts from Theistareykir in the Northern Volcanic Zone (Fig. 1) are the highest degree (*F*) melts, generated at low mean pressure (*P*) of melting, whereas the lavas from the Eastern Volcanic Zone are lower *F* melts produced deeper in the melting region (higher mean *P* of melting; Fig. 4a). The off-rift SP samples have highly variable trace element contents and ratios at a given major element concentration. Compared with the main rift lavas, their higher and much more variable La/Sm and La/Yb ratios (Fig. 4a) indicate a lower extent of melting, whereas their overlapping Fe_2O_3, Lu/Hf and Al_2O_3/TiO_2 imply similar average pressures of melting.

Hf and Nd isotopes

Hf and Nd isotope data are reported in Table 1 and compared with literature Nd–Hf isotope data for Iceland (Salters & White, 1996; Chauvel & Hémond, 2000; Hanan *et al.*, 2000; Kempton *et al.*, 2000; Stracke *et al.*, 2003*c*; Kokfelt *et al.*, 2006; Kitagawa *et al.*, 2008) and the Mid-Atlantic Ridge (Blichert-Toft *et al.*, 2005) in Fig. 5. The rift-zone tholeiites have a restricted range of $^{176}Hf/^{177}Hf = 0{\cdot}28313$–$0{\cdot}28322$ and $^{143}Nd/^{144}Nd = 0{\cdot}51294$–$0{\cdot}51308$. Although there are no systematic distinctions in Hf and Nd isotope compositions between samples from the three main rift areas (RP, WV, NV), samples from the Snæfellsnes Peninsula have the lowest Hf and Nd isotope ratios, whereas those from Theistareykir have the highest ratios. MAR samples generally have higher Hf and Nd isotope ratios compared with the main-rift lavas analysed here, but are similarly or more depleted compared with those from Theistareykir. $^{143}Nd/^{144}Nd$ and $^{176}Hf/^{177}Hf$ in the Icelandic lavas do not correlate with MgO or other fractionation indices (not shown), but are generally correlated with trace element ratios involving a moderately and a highly incompatible element (e.g. La/Sm, La/Yb, Lu/Hf and Sm/Nd; Fig. 6). Correlations between Hf and Nd isotopes and trace element ratios of two highly incompatible elements (e.g. Nb/La, Th/La; Fig. 6c and d), however, are less conspicuous. Whereas the NV and Theistareykir samples form broad systematic trends on diagrams of $^{143}Nd/^{144}Nd$ or $^{176}Hf/^{177}Hf$ versus highly incompatible element ratios, RP and WV samples in particular show a large variability in these elements for a narrow range in $^{143}Nd/^{144}Nd$ and $^{176}Hf/^{177}Hf$.

DISCUSSION

Influence of crustal processes on lava composition

The extent of crystal fractionation and its potential effect on the trace element budget of the magmas is estimated with a least-squares approach using a primitive parent magma composition (Theistareykir sample 9394; Stracke *et al.*, 2003*b*), constant mineral compositions (ol, cpx, plag), and a specific set of mineral–melt partition coefficients (plag: Aigner-Torres *et al.*, 2007; ol: Beattie, 1994; cpx: Hart & Dunn, 1993). The estimated effect on the trace element composition is significant for elements

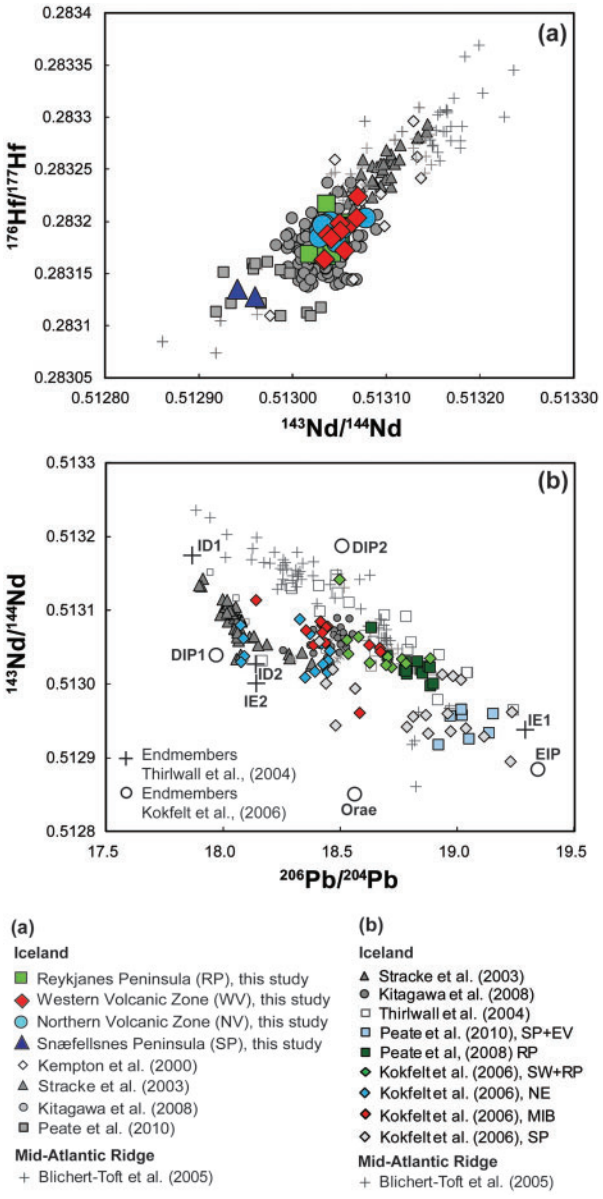

Fig. 5. Variation of $^{143}Nd/^{144}Nd$ vs (a) $^{176}Hf/^{177}Hf$ and (b) $^{206}Pb/^{204}Pb$ for Icelandic samples from this study (a) and from the available literature (b), (see figure legend for references). Samples from the MAR to the north and the south of Iceland (Blichert-Toft *et al.*, 2005) are similar to or more depleted than the most depleted Icelandic samples. Also shown in (b) are previously proposed source components for the Icelandic mantle. Thirlwall *et al.* (2004) suggested two depleted components ID1 and ID2, and two enriched components IE1 and IE2; Kokfelt *et al.* (2006) proposed two depleted components DIP1 and DIP2, one enriched component EIP, and an additional component to explain lava compositions from Oræfajokull Volcano, labelled 'Orae'.

compatible in plagioclase (e.g. Cs, Sr, Eu) whenever plagioclase fractionation exceeds 5%, which affects approximately 90% of the investigated samples. Hence, for example, the Sr concentrations are affected by up to 10% and should be interpreted with care. For the other incompatible elements (e.g. Rb, U, Th, Nb, Ta, REE), however, the effect of fractional crystallization is negligible (i.e. within 1–3% of the concentrations). Trace element ratios such as La/Sm, La/Yb and Lu/Hf are affected by a maximum of 4%, 7·5% and 3·5%, respectively, which is comparable with the analytical reproducibility (2 SD ~3–8%), and insignificant compared with the observed overall variability (70%, 370% and 220%, respectively). Using a different parent magma composition to calculate the proportions of crystallizing minerals does not significantly change the outcome of the least-squares calculations.

Assimilation of the thick, altered Icelandic crust may also affect the geochemical and isotope composition of the lavas (e.g. Oskarsson *et al.*, 1985; Nicholson *et al.*, 1991; Sigmarsson *et al.*, 1992*a*, 1992*b*; Hémond *et al.*, 1993; Gee *et al.*, 1998*b*; Eiler *et al.*, 2000). This process is difficult to resolve owing to the small compositional difference between the recent lavas and the predominantly basaltic Icelandic crust. Meteoric water at the latitude of Iceland has low $\delta^{18}O$ (5·5; Ito *et al.*, 1987; Eiler *et al.*, 1997) compared with typical mantle values (Nicholson *et al.*, 1991; Eiler *et al.*, 2000). Hence low $\delta^{18}O$ in combination with enrichments in K_2O and fluid-mobile trace elements such as Rb or U in evolved, low-MgO (<5 wt % MgO) samples from the Northern (Bindeman *et al.*, 2008) and Eastern Volcanic Zones (Gautason & Muehlenbachs, 1998; Chauvel & Hémond, 2000; Maclennan *et al.*, 2003*a*; Kokfelt *et al.*, 2006) are interpreted to reflect interaction with the altered Icelandic crust. However, crustal assimilation is not expected significantly to influence the geochemistry of the more primitive Icelandic lavas and some studies thus attribute the observed variability in $\delta^{18}O$ largely to mantle source heterogeneity (Gautason & Muehlenbachs, 1998; Chauvel & Hémond, 2000; Skovgaard *et al.*, 2001; Kokfelt *et al.*, 2003, 2006; Maclennan *et al.*, 2003*a*; Stracke *et al.*, 2003*c*). Dredged submarine samples from the Reykjanes Ridge between 63 and 60°N do not pass through thick subaerially altered crust but also have low $\delta^{18}O$ ratios (4·5–5·2‰; Thirlwall *et al.*, 2006). This observation confirms that the low oxygen isotope compositions of Icelandic lavas are indeed a mantle source feature. None of the samples investigated here have anomalous Cs/Rb or K/Rb, suggesting that interaction with crustal fluids and/or the hydrothermally altered Icelandic crust is negligible.

Heterogeneity of the Icelandic mantle

Pb isotope data in combination with Hf, Nd and Sr isotope data from previous studies on young basalts from Iceland's axial rift zone (Hanan & Schilling, 1997; Chauvel & Hémond, 2000; Hanan *et al.*, 2000; Kempton *et al.*, 2000; Thirlwall *et al.*, 2004; Kokfelt *et al.*, 2006; Kitagawa *et al.*, 2008; Peate *et al.*, 2009, 2010) reveal differences in isotope composition between the rift areas. For example, samples

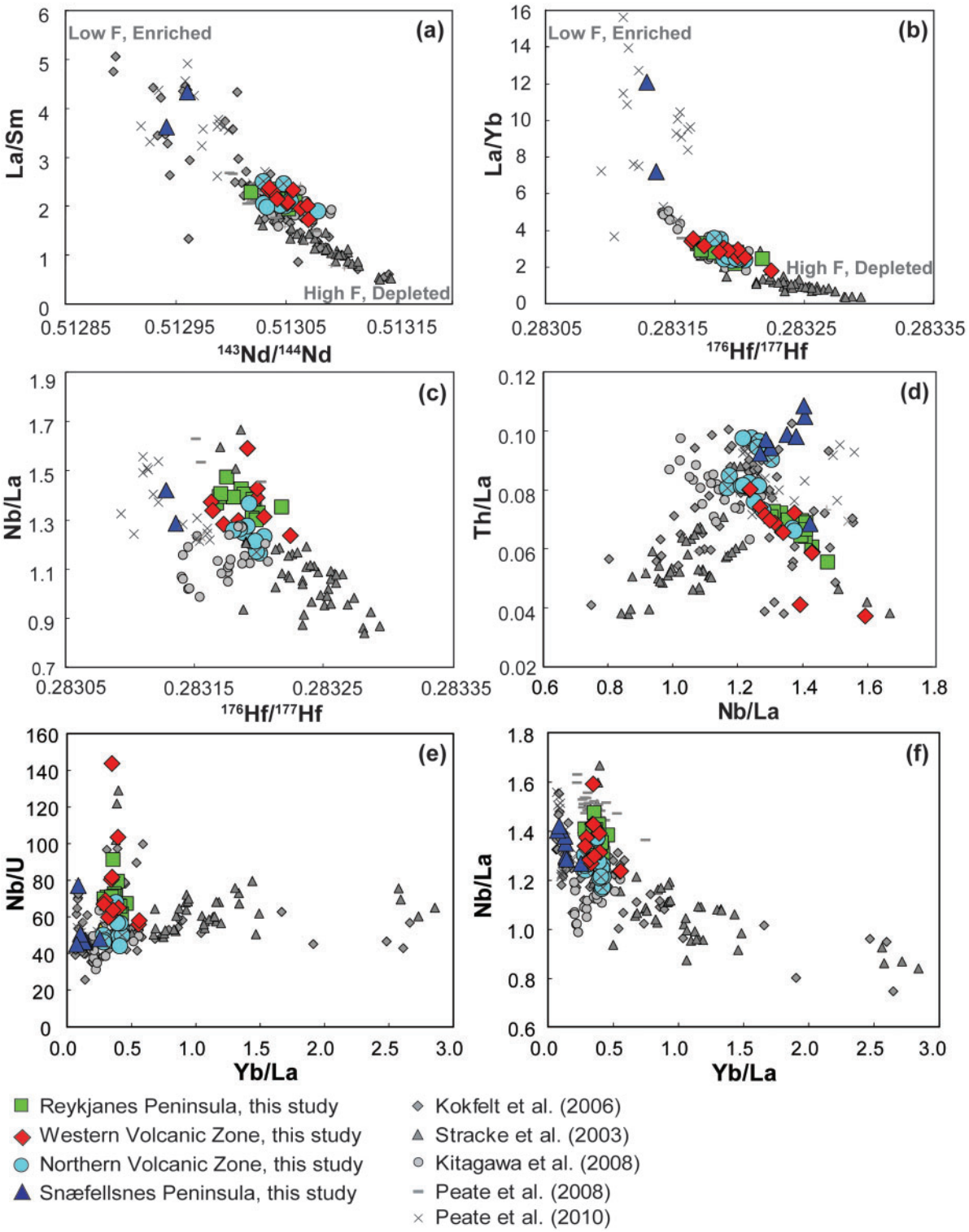

Fig. 6. The relationship between trace element and isotope ratios (a–c) and between various trace element ratios (d–f) in samples from Iceland's rift zones. The Hf and Nd isotope ratios correlate well with trace element ratios involving a moderately incompatible element (a, b), whereas correlations between Hf and Nd isotope compositions and trace element ratios involving two highly incompatible trace elements (c) are poorly defined. RP and WV samples show significant variability in highly incompatible element ratios at a range of $^{143}Nd/^{144}Nd$ and $^{176}Hf/^{177}Hf$. In (e) and (f) the variability of and Nb/U and Nb/La is shown as a function of Yb/La. The samples from the Southwestern rift zones (RP and WV) show a large range in Nb/U and Nb/La at a relatively small range of Yb/La, which suggests mixing with increased proportions of a source that has low U–Th/La but high Nb–Ta/La. Samples with MgO <6 wt % are highlighted with a cross.

from the Western Rift Zone and Reykjanes Rift Zone have more enriched $^{206}Pb/^{204}Pb$ ratios at slightly lower Hf and Nd but more radiogenic Sr isotope compositions compared with samples from the Northern Rift Zone (Fig. 5b). If attributed to mechanical, bulk mixing of end-members, multiple source components are required to explain the full range of isotopic heterogeneity of the Icelandic basalts (Fig. 5b). Peate *et al.* (2010) concluded, however, based on principal component analysis, that >99·5% of the variance in Pb isotope composition in post-glacial Icelandic basalts can be accounted for by mixing between two end-members and that the additional end-members only contribute ~0·5%. Hence the observed isotopic variability in Icelandic lavas can be ascribed to the presence of two main 'genetic' components in the mantle: an enriched component probably represented by recycled oceanic crust and the ambient depleted upper mantle. Assuming the presence of just two components, the variability in $^{206}Pb/^{204}Pb$ ratios within the RP and WV sample groups could arise from mixing with variable proportions of the enriched component (e.g. Hanan *et al.*, 2000) or, alternatively, originate from mixing with an enriched component that is isotopically heterogeneous. It should be noted that we define a component here by its genetic origin rather than by a specific isotope composition. A component is thus created at a given time by a given process (e.g. recycled oceanic crust), and isotopically evolves in isolation. Any initial intrinsic heterogeneity in the trace element composition of such a component is expected to translate over time into isotopic heterogeneity.

Distinguishing the effect of source heterogeneity and fractional melting

Qualitatively, the relative importance of source heterogeneity and partial melting on final melt compositions can be assessed using a combination of isotope and trace element data. Ratios of two trace elements with a large difference in compatibility, such as La/Sm or La/Yb, are sensitive indicators of the degree of partial melting but are, in principle, also controlled by variable source composition. The La/Yb ratio for Iceland varies between 0·35 and 16·6 (this work; Chauvel & Hémond, 2000; Stracke *et al.*, 2003*c*; Kokfelt *et al.*, 2006; Kitagawa *et al.*, 2008) whereas estimates for the La/Yb ratio of the depleted mantle (DM) range from 0·39 to 0·66 (Salters & Stracke, 2004; Workman & Hart, 2005) and La/Yb in MORB, reflecting the compositional range of recycled components, ranges from 0·3 to 3 (Hofmann, 1988; Sun & McDonough, 1989; Su, 2002; Sun *et al.*, 2008; Arevalo & McDonough, 2010). The large variability observed in the Icelandic lavas is therefore probably dominated by variability in the degree of partial melting rather than by variations in source composition. The melting model presented below (see also Table 2 and Supplementary Data Tables IIA and IIB) can be used to illustrate this inference. We assume a heterogeneous source consisting of peridotite (97% of the source) with a La/Yb value of 0·52 that starts melting at 90 km depth and melts to 20%, and a pyroxenite (3% of the source) with a La/Yb value of 0·79 that starts to melt at 100 km and melts to 40%. Mixed melts of this heterogeneous source have La/Yb between 57 at the onset of melting and 0·7 in the final accumulated melts. Hence the variability produced by partial melting is much larger than the difference in composition of the source components. This conclusion holds even if a wider (or narrower) range of possible source components is considered, and supports the notion that large melting-induced variations in La/Sm or La/Yb ratios observed in Icelandic lavas (Figs 4 and 6a, b) are homogenized only to a certain extent by melt mixing during extraction and evolution at crustal levels (Wood *et al.*, 1979; Wood, 1981; Elliott *et al.*, 1991; Slater *et al.*, 2001; Maclennan *et al.*, 2003*a*; Stracke *et al.*, 2003*c*; MacLennan, 2008*a*, 2008*b*).

It should be noted that regional variations in trace element ratios for the main rift lavas are of similar magnitude to the variations observed in the lavas of a single eruptive centre (e.g. Skjaldbreiður in the Western Rift, Table 1, and Theistareykir in the Northern Volcanic Zone; e.g. Fig. 4b). The lack of any systematic geographical variation in trace element ratios along Iceland's rift zones suggests that the compositional variability induced by the local melting and melt extraction process is larger than or similar to regional changes in the melting behaviour expected from the temperature anomaly across the Iceland plume (i.e. higher degree of melting and depth of melt initiation towards the plume centre). As a consequence, the trace element composition of Icelandic basalts cannot be used to detect the inferred progressively lower excess mantle temperature with increasing distance from the plume centre (~100°C, Ribe *et al.*, 1995; Ito *et al.*, 1999; Putirka, 2005; Bourdon *et al.*, 2006).

The systematic relationship between trace element ratios sensitive to the degree of melting, and Hf–Nd isotopic composition indicative of source composition (Fig. 6a and b), can be explained by systematic sampling of two source components as a function of the extent and pressure of melting (Zindler *et al.*, 1979; Elliott *et al.*, 1991; Stracke *et al.*, 2003*c*; Kokfelt *et al.*, 2006; Stracke & Bourdon, 2009). Lavas produced by high degrees of melting (low La/Sm, La/Yb, K_2O) have more depleted isotope signatures (high $^{143}Nd/^{144}Nd$ and $^{176}Hf/^{177}Hf$), whereas samples resulting from low degrees of melting (high La/Sm, La/Yb, K_2O) have enriched isotope signatures (low $^{143}Nd/^{144}Nd$ and $^{176}Hf/^{177}Hf$). This observation indicates that with increasing extent of melting the enriched component becomes progressively diluted. The abundance of the enriched component must therefore be relatively small (a few per cent of the mantle source; Stracke *et al.*, 2003*b*).

Table 2: Compositions of source components

	Peridotite	Pyroxenite*
Cs	0·001	0·014
Rb	0·050	1·188
Ba	0·563	19·32
Th	0·009	0·135
U	0·003	0·046
Nb	0·149	6·130
Ta	0·010	0·351
La	0·190	2·695
Ce	0·550	8·161
Pb	0·018	0·129
Nd	0·581	8·375
Sr	7·664	98·11
Zr	5·082	65·00
Hf	0·157	1·709
Sm	0·225	2·300
Eu	0·096	1·055
Ti	716·0	7558
Gd	0·358	3·700
Dy	0·505	4·400
Y	3·328	24·72
Er	0·348	2·653
Yb	0·365	3·400
Lu	0·058	0·371
$^{87}Sr/^{86}Sr$	0·7027	0·7037
$^{143}Nd/^{144}Nd$	0·5132	0·5127
$^{176}Hf/^{177}Hf$	0·2834	0·2829
$^{206}Pb/^{204}Pb$	17·7	21·2

*The composition of the recycled oceanic crust is calculated by mixing E-MORB 1312-47 (Sun *et al.*, 2008) and average gabbro 735B (Hart *et al.*, 1999) in a 1:1 ratio and applying the dehydration model as presented by Stracke *et al.* (2003*a*), Willbold & Stracke (2006) and Beier *et al.* (2007).

In contrast to trace element ratios that involve a moderately (e.g. Sm, Hf, Yb, Lu) and a highly incompatible element, trace element ratios of highly incompatible elements (i.e. Th, U, Rb, Ba, Nb, Ta, La) approach the source composition at small extents of partial melting and melt mixing. Highly incompatible element ratios in erupted melts from a multi-component source thus represent the weighted average of the compositions of the respective source components (Stracke & Bourdon, 2009). In diagrams of Nb/La vs Th/La or U/La, two striking orthogonal trends are observed for samples from the Northern Volcanic Zone (NV), Theistareykir and the Snæfellsnes Peninsula (SP) on the one hand and samples from the Western Volcanics (WV) and Reykjanes Peninsula (RP) on the other (Fig. 6d). The trend defined by the WV and RP zone lavas require mixing with melts from a source that has high Nb/La and low Th/La. This latter source seems absent in the NV and SP lavas. If the erupted lavas were simple binary mixtures of accumulated melts in a magma chamber, the perpendicular trends in Fig. 6d require mixing of melts from at least three components, similar to what has been suggested based on the combined Pb–Nd–Sr isotope compositions of the WV, RP, and NV samples (e.g. Hanan *et al.*, 2000; Thirlwall *et al.*, 2004; Kokfelt *et al.*, 2006; Peate *et al.*, 2010). This interpretation, however, requires that two of the three components must have very similar $^{143}Nd/^{144}Nd$, $^{176}Hf/^{177}Hf$, La/Yb, and La/Sm ratios to account for the apparent binary mixing relations in Fig. 6a and b.

In a Yb/La vs Nb/La diagram (e.g. Fig. 6f) the NV, Theistareykir and SP data form trends of decreasing Nb/La with increasing Yb/La; that is, increasing extent of melting (F). In contrast, the RP and WV samples have variable Nb/La ratios for a relatively narrow range of Yb/La (0·27–0·55). The variability in highly incompatible elements for the Western Rift Zone (WRZ) and Reykjanes Rift Zone (RRZ) of Iceland compared with the Northern Rift Zone (Table 1) suggests mixing with melts of an enriched component with low (Rb, U, Th)/La but high (Nb, Ta)/La and Nb/U ratios. The most enriched samples (WV26, WV18 and RP6) have Nb/U ranging between 91 and 143 (Fig. 6e), significantly larger than the estimate of 42 ± 1 for Atlantic MORB (Sun *et al.*, 2008). Similar but less extreme enrichments were reported for samples from the RRZ and WRZ by Kokfelt *et al.* (2006) and were ascribed to mixing with a recycled crust component. It should be noted that despite the large variability in highly incompatible trace element ratios for the WV and RP samples, their Yb/La value is relatively constant (Fig. 6e), suggesting a comparatively constant degree of melting.

For Iceland the relationships between the Hf and Nd isotopic compositions and La/Yb or La/Sm are consistent with partial melting and progressive mixing of melts from two components. In the following discussion we therefore investigate whether a two-component polybaric melting and melt mixing model can reproduce the full range of trace element and Pb–Hf–Nd–Sr isotopic heterogeneity in Icelandic basalts, or whether more than two mantle source components are required. We test two melt mixing scenarios: (1) complete mixing of all melts generated in the melting region for variable proportions of the enriched and depleted source components; (2) incomplete mixing of melts from a source with a constant proportion of the enriched and depleted source components.

Partial melting of a heterogeneous source and melt mixing

The nature and location of melt mixing

The large variability in trace element ratios in Icelandic basalts and associated melt inclusions suggests that the melts are not efficiently mixed before eruption (Gurenko & Chaussidon, 1995; Slater *et al.*, 2001; Maclennan *et al.*, 2003*b*; MacLennan, 2008*a*, 2008*b*). However, the trace element compositions of predicted instantaneous melts formed near the base of the melting region are much more extreme than those of the main rift lavas (e.g. MacLennan, 2008*a*), indicating that a certain extent of mixing of these fractional melts with melts formed at lower pressures is required. In addition, melt extraction without continuous equilibration with the ambient mantle (i.e. channelized melt transport) is required to explain the compositional variability observed in the melt inclusions (Gurenko & Chaussidon, 1995; Slater *et al.*, 2001; Maclennan *et al.*, 2003*a*; MacLennan, 2008*a*, 2008*b*) and the preserved U-series disequilibria (Kokfelt *et al.*, 2003; Stracke *et al.*, 2003*b*, 2006). Because of the apparent greater role of melt mixing within the high-porosity melt channels, compared with mixing during fractional crystallization at shallow mantle or crustal levels (Maclennan *et al.*, 2003*a*; Maclennan, 2008*b*), we focus here on modelling melt mixing during melt extraction from the mantle.

Modelling melting and mixing of a heterogeneous source

During fractional melting of a heterogeneous mantle source, the final trace element and isotopic composition of the erupted melts depend on: (1) the composition of the source components involved; (2) the difference in melting and trace element partitioning behaviour of the source components; (3) the relative mass fractions of the source components; (4) the style of melt mixing during partial melting and melt extraction.

Partial melting of a compositionally heterogeneous mantle is approximated by polybaric melting and systematic sampling and mixing of melts from two source components, a depleted peridotite and an enriched pyroxenite (see Figs 7 and 8, Table 2; and Stracke & Bourdon, 2009). Fractional melting is simulated by incremental 'dynamic melting'; that is, by small steps of batch melting while keeping a small melt fraction (0·1%) residual [for a detailed description of the model see Stracke *et al.* (2003*b*)]. The amount of melt extracted at each step is constant and depends on the total degree of melting F and the number of melting increments (1000). The compositions of the instantaneous and accumulated peridotite and pyroxenite melts along the melting trajectories are calculated separately and the instantaneous melts are mixed and accumulated in different ways (see Fig. 7). The compositions of the mixed melts as a function of depth of melt extraction are illustrated in Figs 9–11. The model input parameters are

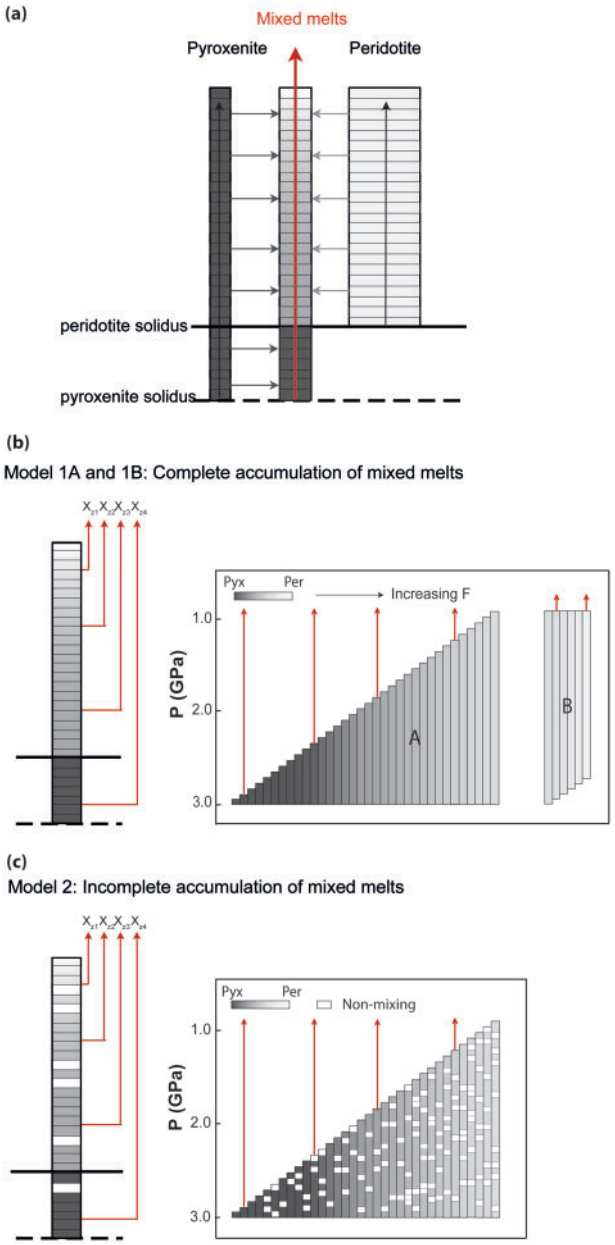

Fig. 7. Schematic representation of the melting and melt mixing models. (a) Two source components, a peridotite (light grey) and a pyroxenite (dark grey), are melted using two separate polybaric melt models implementing the different melting behaviour of the sources (Supplementary Data Tables IIA and IIB). Partially accumulated melts packages, integrated over 1 km depth intervals, from both sources are mixed according to their relative mass proportions (see text). (b, c) Two styles of melt accumulation of the pre-mixed melt batches are considered. Models 1A and 1B simulate complete accumulation of all melt batches but extraction of the melts from variable depths (i.e. variable lengths of the melt columns; see main text); model 2 simulates incomplete accumulation, where 20% of the melt batches (represented by blank melt increments) do not mix. For both models the compositions of melts for every 1 km depth of melt extraction are calculated (e.g. x_{z1}, x_{z2} and x_{z3} represent compositions of melts extracted from depths z_1, z_2 and z_3). Compositions of mixed melts for these models are shown in Figs 9–11.

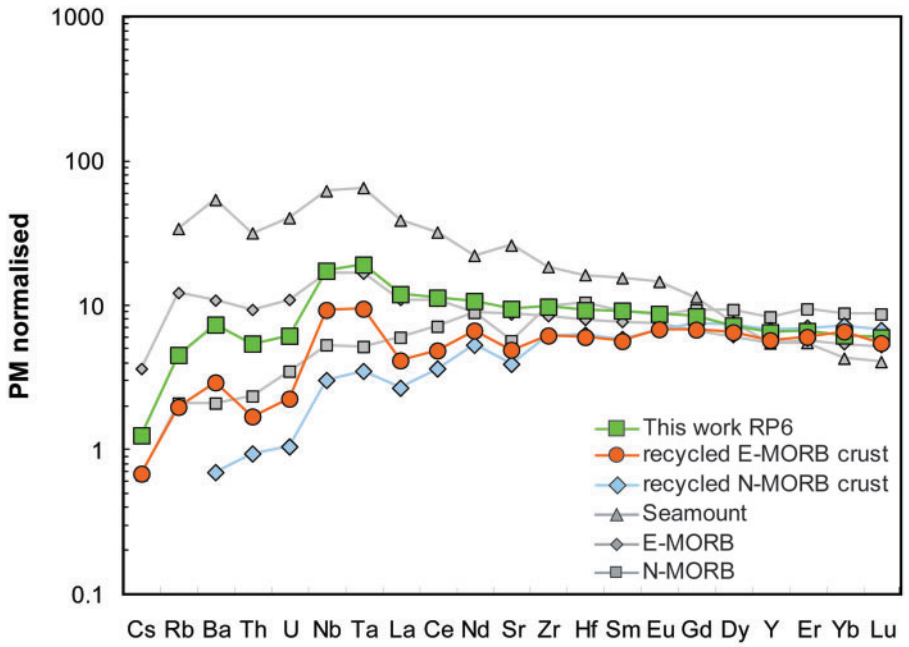

Fig. 8. Primitive Mantle (PM) normalized trace element patterns of possible enriched source components compared with a representative Icelandic basalt (sample RP6). E-MORB and RP6 (unlike N-MORB) are similarly enriched in Nb and Ta relative to the neighbouring elements (Th, U and La). Recycled E-MORB crust, consisting of 50% E-MORB and 50% gabbro that has been modified during subduction (Stracke *et al.*, 2003*a*) has a similar multi-element pattern to sample RP6. It should be noted that the absolute effect of the subduction modification is poorly constrained quantitatively (Ayers *et al.*, 1997; Kogiso *et al.*, 1997; Johnson & Plank, 1999; Hermann *et al.*, 2006; Melekhova *et al.*, 2007; Klimm *et al.*, 2008) and that the composition of E-MORB is highly variable. The E-MORB composition represents sample 1312-47 from Sun *et al.* (2008); gabbro in the recycled crust is from Hart *et al.* (1999); the seamount is sample Nintoku 55-8 from Regelous *et al.* (2003); N-MORB is from Hofmann (1988). The recycled N-MORB crust represents the enriched component used in the polybaric melting and mixing model of Stracke & Bourdon (2009).

listed in Table 2, Fig. 8 and Supplementary Data Appendix Tables IIA and IIB.

The model presented here differs from conventional mixing models in that it mixes accumulated melts from two sources with different solidii and melt functions during the extraction process (see also Phipps Morgan, 1999; Ito & Mahoney, 2005) rather than mixing final batches of melts integrating over the entire melting column or mixing bulk source end-member compositions (e.g. Chauvel & Hémond, 2000; Hanan *et al.*, 2000; Thirlwall *et al.*, 2004; Kokfelt *et al.*, 2006; Kitagawa *et al.*, 2008; Maclennan, 2008*b*).

Input composition of source components

The enriched pyroxenite component used in the model calculations is 2 Ga recycled oceanic crust modified during the subduction process by dehydration (Table 2, Fig. 8; Stracke *et al.*, 2003*a*). Such a component has been inferred to be the enriched component in the Icelandic mantle source (e.g. Chauvel & Hémond, 2000; Stracke *et al.*, 2003*c*; Kokfelt *et al.*, 2006) as its composition matches the observed depletion in Ba, Rb, U, and Th and the enrichment in Nb and Ta compared with La in Icelandic lavas. The strong enrichment in Nb and Ta relative to the neighbouring highly incompatible elements in the most enriched basalt samples from this study (i.e. RP6 has Nb/La of 1·5; Fig. 8) suggests that the enriched component could indeed represent recycled enriched MORB (E-MORB, as suggested by McKenzie *et al.*, 2004). In general, E-MORB and seamount samples are characterized by strong fractionations between Nb and Ta and the neighbouring elements (La, U, Th; Fig. 8; Zindler *et al.*, 1984; Niu & Batiza, 1997; Regelous *et al.*, 2003; Sun *et al.*, 2008). However, the absolute fractionation between the highly incompatible elements in E-MORB and seamount basalts is still less pronounced compared with our most enriched RP and WV lavas. Applying a dehydration model (for parameters see Stracke *et al.*, 2003*b*; Willbold & Stracke, 2006, 2010; Beier *et al.*, 2007; Willbold *et al.*, 2009) to a crust consisting of 50% E-MORB (sample 1312-47; Sun *et al.*, 2008) and 50% gabbro (Hart *et al.*, 1999) decreases the Rb, U, Th and La compared with Nb and Ta and yields a recycled component with similar Rb/La, U/La, Nb/La, and U/Nb to our most enriched samples (Table 2, Fig. 8). Isotope compositions for the 2 Ga recycled E-MORB component are calculated following the approach from Stracke *et al.* (2003*a*). The depleted component in the model represents average depleted mantle (see Table 2; Stracke *et al.*, 2003*a*; Salters & Stracke, 2004; Workman & Hart, 2005).

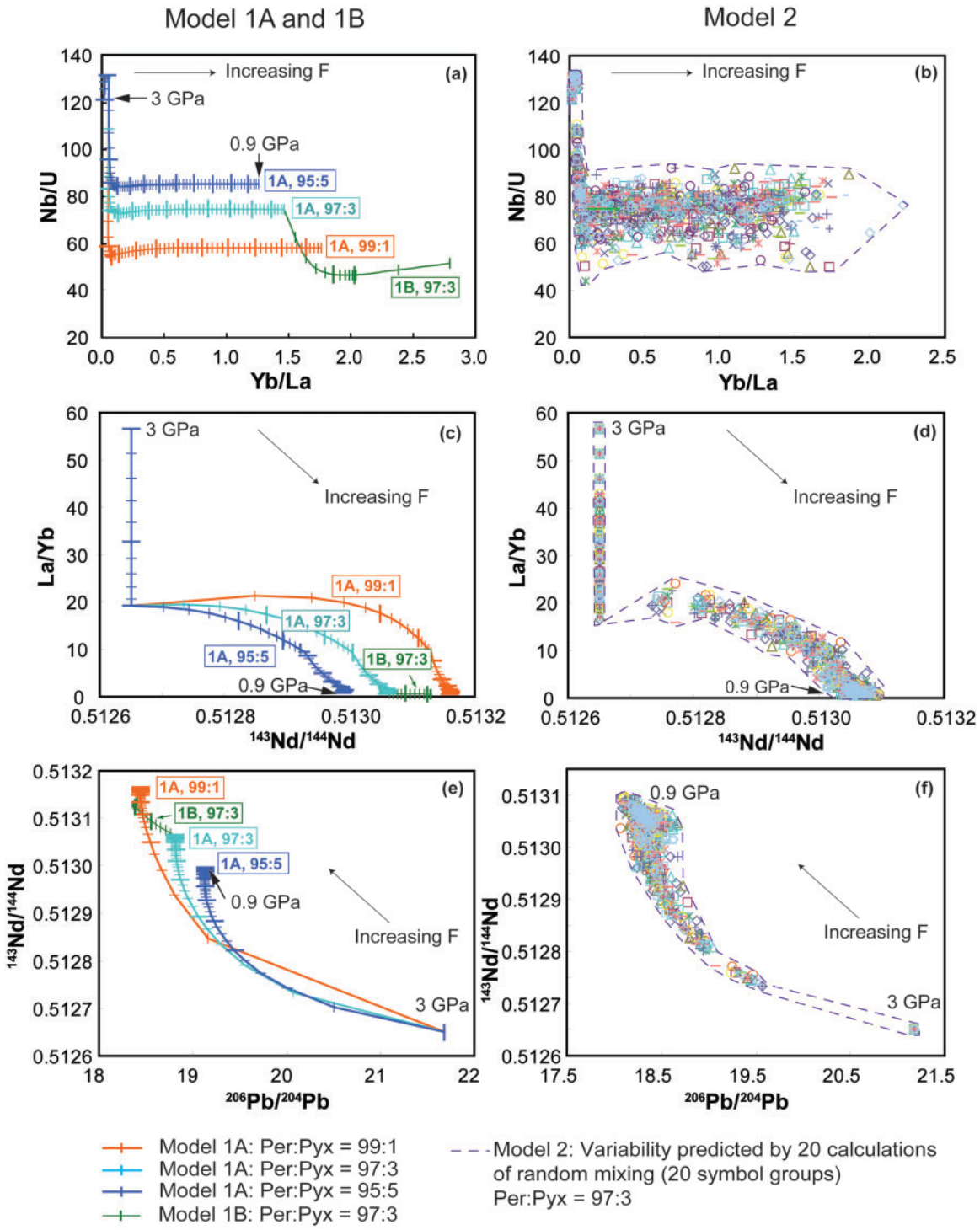

Fig. 9. Presentation of the mixing model results in diagrams of Yb/La vs Nb/U, $^{143}Nd/^{144}Nd$ vs La/Yb, and $^{206}Pb/^{204}Pb$ vs $^{143}Nd/^{144}Nd$. Left panels (a, c, e) show calculated trends for model 1A, complete mixing of melts integrated over variable depth intervals for a constant initial, but variable final pressure of melting, and model 1B, where melts are integrated over variable depth intervals assuming a constant final depth of melting (0·9 GPa) but a variable initial depth of melting (initial peridotite–pyroxenite ratio of 97:3). The different trends plotted for model 1A represent variable proportions of the pyroxenite component relative to the peridotite component (see legend and labels). Small tick marks represent pressure intervals of 0·03 GPa (1 km); large tickmarks 0·15 GPa (5 km). The panels on the right (b, d, f) show results of model 2. Each symbol group represents the compositions of melts extracted from the entire depth range calculated for one randomly assigned mixing probability. Altogether, results for a series of 20 calculations for random mixing and extraction from variable depths are shown (20 symbol groups). The total variability predicted from these 20 calculations is represented by the shaded field. (For a detailed description of all model calculations, see the main text.)

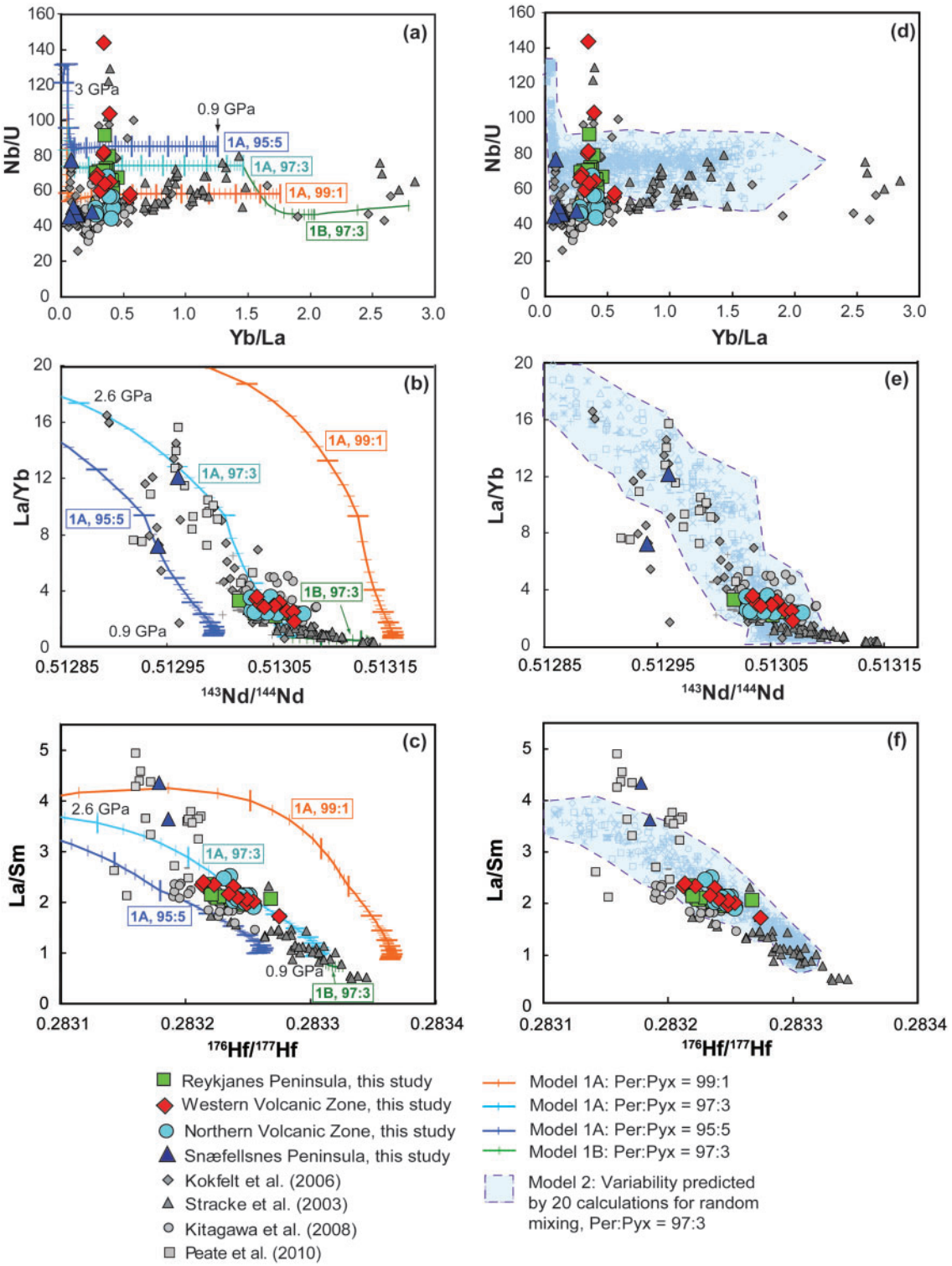

Fig. 10. Comparison of the model calculations presented in Fig. 9 with trace element and isotope data for Icelandic basalts. In (a), (b), and (c) we compare the calculated compositions for model 1A and model 1B with the data. In (d), (e), and (f) we compare compositions from model 2 (open symbols and shaded field) with data for Iceland. (For a detailed description of all model calculations and discussion, see the main text and the caption of Fig. 9.) Literature data sources are listed in the legend.

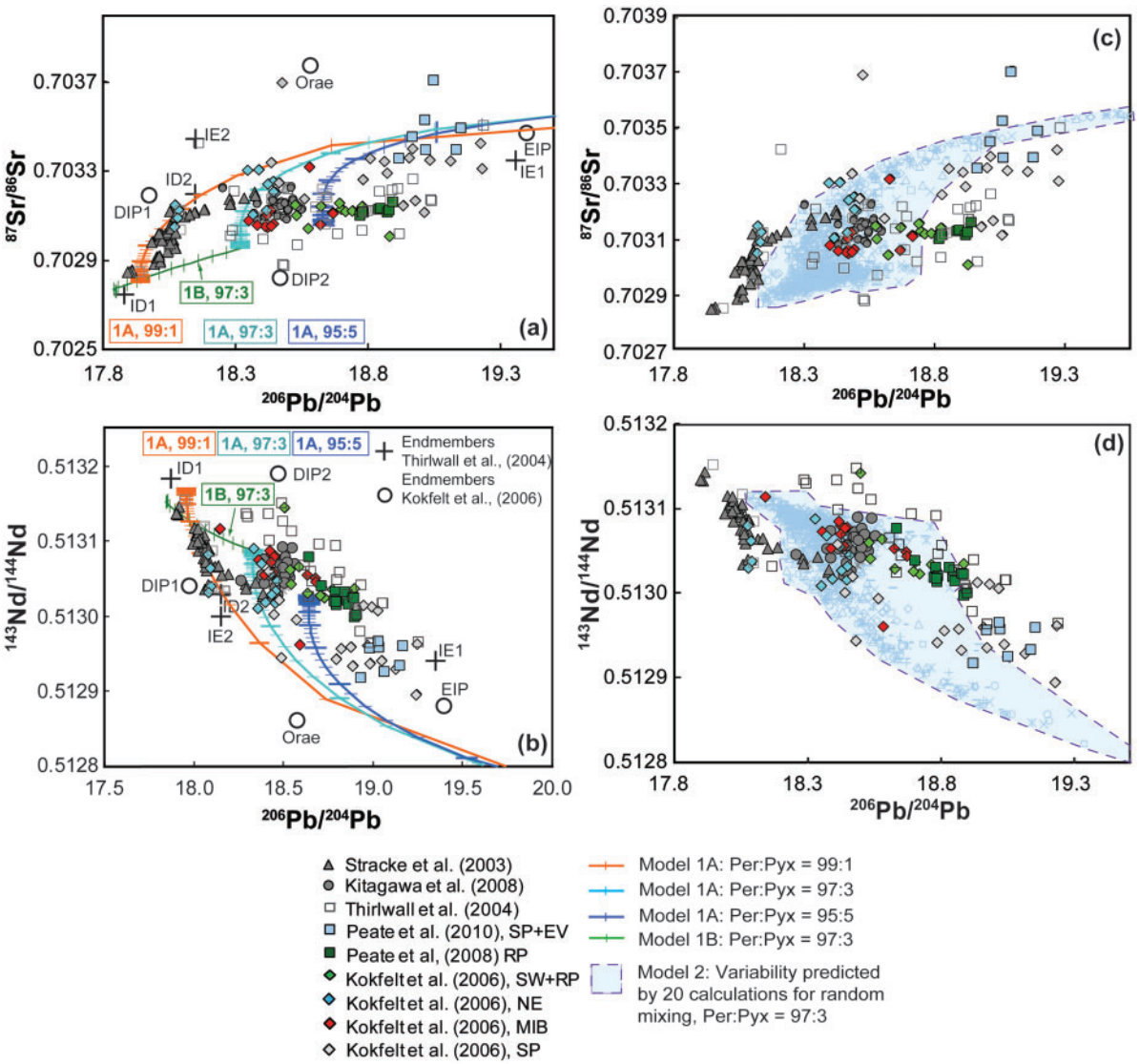

Fig. 11. Comparison of model calculations presented in Fig. 9 with Nd–Pb and Sr–Pb isotope literature data for Icelandic basalts. In (a) and (b) we compare the calculated compositions for model 1A and model 1B (see legend and labels). In (c) and (d) we compare results for model 2 (open symbols and shaded field) with literature data for Iceland. In (a) and (b) the mantle source components as suggested by Thirlwall *et al.* (2004) and Kokfelt *et al.* (2006) are also shown for comparison (see also Fig. 5b). (For a detailed description of all model calculations and discussion, see the main text and the caption of Fig. 9.) Literature data sources are listed in the figure legend.

Melting behaviour of the source components

Pyroxenite and peridotite have different melting behaviours (e.g. Hirschmann *et al.*, 1999; Pertermann & Hirschmann, 2003). These differences can enhance the variability in melt composition during melting of a heterogeneous source (Stracke & Bourdon, 2009). Pyroxenite solidus temperatures have been determined to range from being similar to that of peridotite to ~250°C lower than that of peridotite at a given pressure (Hirschmann *et al.*, 2003; Pertermann & Hirschmann, 2003; Kogiso *et al.*, 2004). Melting of pyroxenite is therefore expected to start at similar or higher pressures compared with the peridotite. Slightly deeper melt initiation for pyroxenite compared with peridotite (i.e. 100 km vs 90 km) is assumed here, which is consistent with the solidus temperature determined for E-MORB-like MIXlG by Hirschmann *et al.* (2003). A small difference in solidus temperature between the two source components is also consistent with the observed enrichment in La/Yb and La/Sm in the most enriched Icelandic lavas (see Stracke & Bourdon, 2009). The maximum degree of melting over the full melting interval is 20% for the peridotite, whereas it is assumed to

be 40% for the pyroxenite. Melt productivity, defined as the amount of melt generated for a given decrement of pressure during adiabatic upwelling (dF/dP), is different for the peridotite and pyroxenite. The polybaric melt productivity function of Pertermann & Hirschmann (2003) is implemented for the pyroxenite and the melt productivity function of Asimow *et al.* (2004) for the peridotite. The relative contributions of the peridotite and the pyroxenite melts vary as a function of the degree of melting and the initial abundance of the two components at the onset of melting.

Styles of melt aggregation and mixing

Two 'styles' of mixing and melt accumulation were adopted to model the full range of highly depleted (Theistareykir) to highly enriched (off-rift) Icelandic melt compositions: complete mixing (model 1) and incomplete mixing (model 2, see Figs 7, 9, 10 and 11). Model 1A simulates complete mixing of all instantaneous melts and integration of the accumulated melts over various depths in the melting column, assuming a constant initial pressure of melting but a variable final depth of melt extraction (following Stracke & Bourdon, 2009). Different melt column lengths in this model (Fig. 7) thus represent different overall extents of melting with different absolute and relative proportions of peridotite- and pyroxenite-derived melts. In this respect, model 2 is similar to model 1A, but model 2 assumes incomplete and random mixing of instantaneous melts in a given melting column (Fig. 7). In addition, we tested a scenario where complete mixing of melts in a given melt column occurs, as in model 1A, but with the difference that melts are extracted from a constant final depth, but variable initial depth of melting (model 1B in Fig. 7). In model 1B, variable melt column lengths result from truncating the bottom of the melting column rather than the top as in model 1A. Such a scenario was suggested by Elliott *et al.* (1991) to explain the highly depleted nature of picrites from Theistareykir and the Reykjanes Peninsula.

For simplicity, instantaneous melts in models 1A, 1B and 2 are accumulated over 1 km (= 0·03 GPa) intervals to obtain single peridotite and pyroxenite 'melt packages', which are then subsequently mixed to obtain the compositions of pre-mixed melt batches, taking into account their relative mass proportions. The mass proportions of the peridotite and pyroxenite melt packages are a function of the amount of melt formed in the 1 km pressure intervals (dF/dz) and of the abundance of the two components at the onset of melting:

$$M_{\mathrm{PER}}(\mathrm{z}) = \mathrm{d}F/\mathrm{d}z_{\mathrm{PERz}} \times 1\mathrm{km}(z) \times Ab_{\mathrm{PER}};$$
$$M_{\mathrm{PYX}}(\mathrm{z}) = \mathrm{d}F/\mathrm{d}z_{\mathrm{PYXz}} \times 1\mathrm{km}(z) \times (1 - Ab_{\mathrm{PER}})$$

where Ab_{PER} is the fraction of peridotite in the source (e.g. 97%). The pre-mixed melt batches are subsequently accumulated in different ways; that is, complete accumulation in models 1A and 1B, and incomplete accumulation in model 2 (Fig. 7), leaving out 20% of the mixed melt batches in a random fashion.

To model incomplete mixing, we used a function based on a random number generator to simulate a certain probability of mixing (p). This function yields the value of the 'mixing factor' (b) for every depth, which is equal to 1 if the melt batch mixes and equal to 0 if the melt batch does not mix. For the calculations presented here (Figs 7, 10 and 11), the probability of mixing for each melt batch is assumed to be 0·8 (i.e. the chance that the pre-mixed melt batches mix is 80%). The final compositions of the incompletely aggregated melts at any depth (i.e. every 1 km of melt extraction) are calculated using the equation

$$\bar{X}_i(z) = \sum_{j=1}^{n} (x_{ij} \times f_j \times b_j)$$

where X_i is the composition of the final accumulated melt for element i calculated at depth z of melt extraction, j represents the mixed melt increment and varies from unity at depth $z_0 = 100$ km to n at the final depth in the melt column, x_{ij} is the concentration of element i in the mixed melt increment j, f_j is the relative mass fraction of the melt batch $[f(z) = (M_{\mathrm{PERj}} + M_{\mathrm{PYXj}})/M_{\mathrm{Total}}]$ and b_j is the mixing factor that is assigned for each melt batch by the random number generator (i.e. $b_j = 1$ or 0). The total mass fraction is determined for each depth of melt extraction and every random calculation by

$$M_{\mathrm{Total}} = \sum_{j=1}^{n} (f_j \times b_j).$$

A possible physical reason for incomplete accumulation of melts in model 2 may be that melts from different parts of the drainage system are extracted at different times and thus feed different eruptions. It should be noted that melts are extracted from the residue only after a certain threshold porosity is reached. The threshold porosity for any depth in the melt region may not be reached simultaneously, which may result in instantaneous melts from certain depths mixing whereas others do not.

The calculated model trends are presented in Fig. 9 for three initial proportions of the depleted and enriched component, 99:1, 97:3 and 95:5, for model 1A (panels a, c and e) and for a constant initial peridotite:pyroxenite ratio of 97:3 for models 1B and 2 (panels b, d and f). For model 2 a series of 20 random calculations, excluding 20% of the melts in each series, but extracted from all depths, were performed.

Comparison of observations and model results

A comparison of the model results with the Iceland data is shown in Figs 10 and 11. Generally, the results obtained

from model 2 encompass almost the entire range of observed compositions for a constant ratio of the enriched and depleted source component (3:97). In contrast, a variable abundance of the enriched component is required for complete overlap of the observed data and calculated data from model 1A.

Main rift lavas

Accumulation and extraction of fully mixed melts with degrees of melting up to 10% for the peridotite and 20% for the pyroxenite (i.e. accumulation over 40 km) is consistent with the variability in Yb/La for the main rift lavas (i.e. RP, WV and NV; Fig. 10a). For this scenario (model 1A), however, the different enrichments in highly incompatible elements (i.e. high Nb/U and high Nb/La) for samples from the Reykjanes Rift Zone and Western Rift Zone and the Northern Volcanic Zone, respectively, require that the enriched source component is more abundant (i.e. 2·5–10%; Fig. 10a) beneath the Reykjanes and Western Rift Zone compared with the Northern Rift Zone (0·5–1%). The enrichments in Nb and Ta compared with La and U in the most enriched RP and WV samples are, however, more extreme than calculated with model 1A, even for large (e.g. 50%) initial proportions of the enriched component. This observation suggests that the enriched component may have even higher Nb,Ta/La,U ratios than assumed in the calculation (Table 2, Fig. 8) or that the enriched component is intrinsically heterogeneous in trace element composition, which is not accounted for by the model.

In diagrams of $^{143}Nd/^{144}Nd$ vs La/Yb or $^{176}Hf/^{177}Hf$ vs La/Sm (Fig. 10b and c) the samples most enriched in highly incompatible elements from the RRZ and WRZ do not have significantly lower Hf and Nd isotope ratios than the lavas from the NRZ as predicted by model 1A for larger proportions of the enriched component (5–10%). This observation suggests either a slight misfit of the Hf and Nd isotopic compositions of the model end-members (Table 2) or that the abundance of the enriched component is in fact constant across Iceland.

Incomplete mixing of melts from a source with a constant initial peridotite:pyroxenite ratio (97:3, model 2) results in significant variability in highly incompatible trace elements that adequately accounts for the observed variability in the main rift data (Fig. 10d–f). A large portion of the scatter observed in the data results without having to assume variable abundances of the enriched component underneath each of the rift zones.

It should be noted that the variability in highly incompatible trace element contents of the accumulated melts in model 2 is highly sensitive to the extent of mixing with the highly enriched initial pyroxenite melts from the bottom of the melting column. For example, when the initial pre-mixed melt batches from between 100 and 98 km depth are not included in the final mixture, its composition is significantly more depleted (mixed melt compositions with low Nb/U in Fig. 10d). Highly enriched compositions arise from model 2 when all of the enriched deep melt batches are mixed in but melts formed at shallower depths in the melting region are excluded. Decreasing the probability of mixing results in an increase of the variability in the accumulated melt compositions and vice versa. Less efficient mixing of melts as assumed in the model (i.e. $p < 0{\cdot}8$) could therefore explain the larger variability observed in highly incompatible element ratios in some of the WV and RP samples.

Theistareykir lavas

The highly depleted Theistareykir samples with low La/Yb (down to 0·5), and high Nd and Hf isotope ratios require accumulation of melts over a large depth range (40–70 km) with degrees of melting >20% for the most depleted picrites (Fig. 10a and b; Stracke *et al.*, 2003*c*). Equally depleted high-degree melts are observed as picrites from the Reykjanes Peninsula, which are similar to the Theistareykir lavas erupted in early post-glacial times (10–8 ka; Jakobsson *et al.*, 1978; Gee *et al.*, 1998*a*, 1998*b*; Maclennan, 2008*b*). This observation suggests that about 10 kyr ago melting was more extensive, which is attributed to increased melt productivity during concurrent isostatic rebound and unloading of ice sheets (Jull & McKenzie, 1996; Gee *et al.*, 1998*a*; Maclennan *et al.*, 2002). The larger variability in trace element and isotope ratios for the Theistareykir lavas (Slater *et al.*, 2001; Maclennan *et al.*, 2002, 2003*a*; Stracke *et al.*, 2003*c*; McKenzie *et al.*, 2004) compared with the other main rift lavas can therefore be explained assuming a larger depth interval of melt extraction relative to other areas along the rift. If the depth range of melt accumulation for the Theistareykir lavas is assumed to be similar to that of the main rift lavas, the peridotite melting rate, or melt productivity (dF/dP), has to be a factor of two higher. It should be noted, however, that it is more likely that the amount of melt generated during early post-glacial times varied as a result of changes in mantle upwelling velocity, a variable that is not accounted for by our melting model.

Alternatively, Elliott *et al.* (1991) suggested that the highly depleted nature of the picritic Theistareykir and Reykjanes Peninsula magmas could result from a lack of mixing with the most enriched melts from the deeper part in the melting column. Higher proportions of melts from shallow depths as a result of glacial unloading were also predicted by the model of Jull & McKenzie (1996).

Model trends that lack the most enriched deep instantaneous melts (model 1B, Figs 9a, c, e, and 10a, b, c) show that this process can indeed generate the highly depleted trace element and Nd and Hf isotopic compositions of the picritic lavas, assuming that the source contains 3% pyroxenite. This scenario requires a mechanism to exclude a large portion of the initial highly enriched melts from

mixing with the more depleted melts formed at higher levels in the melt region. Younger post-glacial lavas would perhaps be expected to have enriched signatures complementary to those of the depleted lavas, assuming these would include the bottom melts previously left out.

Off-rift lavas

The off-rift samples have high but variable incompatible trace element concentrations and ratios (e.g. La = 9–27 ppm and La/Yb = 4·0–14·3) and low Nd and Hf isotope compositions. These compositions are matched by mixing small degree melts (peridotite $F = 1$–3%, pyroxenite $F = 1$–10%) from deep in the melting region and accumulation over a limited depth range (~25 km) compared with samples from the main rifts (~40 km, La = 2·8–17·0 ppm and La/Yb = 1·8–3·6, Fig. 10a). The generally smaller degree of melting can be explained by the presence of a lithospheric lid whose thickness increases away from the ridge and restricts the final depth of melting to greater depths compared with the main rift lavas (Kokfelt *et al.*, 2006; Peate *et al.*, 2010). Variability in Nd isotope composition for the off-rift lavas requires variable proportions of the enriched component in the source (~3–5%) in model 1A, but is equally well matched by incomplete mixing of melts and extraction of these partial accumulated melts from variable depths (model 2, Fig. 11).

Pb–Sr–Nd isotope variability in Iceland

As for the highly incompatible trace element ratios, the combined Nd–Sr–Pb isotope compositions of Iceland's main rift and off-rift lavas (Fig. 11a and b; Hanan & Schilling, 1997; Chauvel & Hémond, 2000; Hanan *et al.*, 2000; Stracke *et al.*, 2003*c*; Thirlwall *et al.*, 2004; Kokfelt *et al.*, 2006; Kitagawa *et al.*, 2008; Peate *et al.*, 2009, 2010) are reproduced by complete accumulation, as in model 1A, but require variable initial abundances of the enriched component for different ridge segments. A small proportion (1%) of the enriched component in the source is required to match the data for Theistareykir and other samples from the Northern Volcanic Zone (low $^{206}Pb/^{204}Pb$ and slightly higher $^{143}Nd/^{144}Nd$) and can also explain the off-rift lavas, which result from smaller degrees of melting and have relatively low $^{143}Nd/^{144}Nd$. It should be noted that the most depleted Theistareykir melts are also matched by model 1B, which assumes exclusion of the most enriched melts from the deeper part in the melting column, with 3% of the enriched component (Fig. 11a and b). The higher and more variable $^{206}Pb/^{204}Pb$ data for the Western Rift Zone and Reykjanes Peninsula lavas demand a higher proportion of the enriched component of 3 to ~15% (Fig. 11a and b) similar to what has been observed for the incompatible trace element ratios.

Model 2, incomplete mixing of melts, produces melts with significant isotopic variability covering a large part of the Icelandic data range for a constant initial abundance of the two source components (Fig. 11c and d). Only a few samples, which have high $^{143}Nd/^{144}Nd$ compositions at a given $^{206}Pb/^{204}Pb$, reported by Thirlwall *et al.* (2004), are not satisfactorily explained by the model. Data points that lie out of the predicted range can, however, be explained by the end-members themselves being heterogeneous with respect to their trace element and isotope composition.

In summary, the observed enrichments in Nb and Ta compared with U and La, as well as the high $^{206}Pb/^{204}Pb$ and $^{87}Sr/^{86}Sr$ isotope composition for WV and RP samples compared with NV and Theistareykir samples, can be explained by both complete and incomplete accumulation of melts. Model 1A, complete accumulation of mixed melts, requires a greater abundances of the enriched source component beneath the Reykjanes Peninsula and the Western Rift Zone, whereas model 2, incomplete accumulation of melts from the two source components, can explain the variability in highly incompatible trace elements and Hf–Nd–Sr and Pb isotope compositions with a constant abundance ratio of the source components across Iceland. It should be noted that the small range in Hf and Nd isotope compositions for the most enriched WV and RP samples is difficult to reconcile with a higher abundance of the enriched component, which makes model 2 the more likely scenario.

Compared with the actual process, the mixing model applied here is highly simplified. Melt extraction from the mantle is poorly understood, but is likely to be a complex process in which melts transported in multiple channels converge at various levels into wider channels (Hart, 1993). The better match of the Icelandic data to the results of model 2 implies that mixing and extraction of melts formed from various depths is stochastic and that separate eruptions therefore integrate melts produced in different parts of the melting region. Importantly, however, the results presented above show that the way melts from different source components mix during progressive melting has a large effect on the trace element and isotope composition of the final erupted melts and may obviate the apparent need for multiple source components inferred from bulk-source mixing models (e.g. Hanan & Schilling, 1997; Chauvel & Hémond, 2000; Hanan *et al.*, 2000; Stracke *et al.*, 2003*c*; Thirlwall *et al.*, 2004; Kokfelt *et al.*, 2006; Kitagawa *et al.*, 2008; Peate *et al.*, 2009).

Intrinsic heterogeneity of the enriched component

As an alternative to the scenarios discussed above, intrinsic heterogeneity of the enriched source component may account for some of the compositional differences observed between the WRZ, RRZ and NRZ lavas. Assuming the enriched component represents recycled oceanic crust, the intrinsic trace element heterogeneity of its constituents, basalts and gabbros, perhaps increased or amplified by non-uniform dehydration during subduction, could

account for regional differences in the enriched component across the Icelandic rift zone.

Peate *et al.* (2010), suggested that mixing with a third (and/or fourth) component beneath Iceland results in the subtle shift from the binary array in a $^{208}Pb/^{204}Pb$ vs $^{206}Pb/^{204}Pb$ diagram, causing a kinked trend for the Icelandic data. Instead of having more than two components, however, the subtle variability in Pb isotopes could result from the enriched component being intrinsically heterogeneous. The component sampled by lavas in the Eastern Volcanic Zone is more enriched in $^{206}Pb/^{204}Pb$ compared with the component present beneath the Northern Volcanic Zone. If the radiogenic Pb component represents recycled oceanic crust, intrinsic heterogeneity in Pb isotopic composition could be explained by initial heterogeneity in Th, U and/or Pb concentrations. Assuming an age for the recycled crust of 2 Ga, an initial heterogeneity in U content of 4% would be sufficient to result in an offset in $^{206}Pb/^{204}Pb$ between the Eastern and Northern Volcanic Zone ($\Delta^{206}Pb/^{204}Pb \sim 0{\cdot}2$) as observed in the $^{208}Pb/^{204}Pb$ vs $^{206}Pb/^{204}Pb$ diagram (Peate *et al.*, 2010, fig. 9b). Variability in Pb concentration of 5% in the enriched component could equally result in the diversity observed in Icelandic basalts between the ERZ and NRZ. Such variability in Pb or U concentration is small compared with the variability in U in present-day MORB (Sun *et al.*, 2008). Thus, if intrinsic heterogeneity in U and Pb in the enriched component is considered, two components suffice to explain the variability of Pb isotope compositions in Iceland.

CONCLUSIONS

The large compositional variability observed in the post-glacial lavas from Iceland can be explained by melting of only two components in the Iceland mantle source, if the effects of melt mixing during extraction from the mantle are considered.

Two styles of melt mixing and accumulation were considered: (1) complete accumulation of all melts and extraction of the mixtures from variable depths; (2) incomplete accumulation of melts where 20% of the melts are excluded in a random fashion. Both models adequately reproduce the compositional variability observed in Icelandic basalts by melting a two-component source consisting of a depleted mantle source that contains small amounts (1–10%) of an ancient enriched E-MORB-like recycled crust. However, to explain the compositional variability between lavas from the Northern and the Southwestern Rift Zones by complete accumulation (model 1A), the abundance of the enriched component beneath the latter zone must be larger, or, alternatively, the enriched component is slightly heterogeneous in composition. Initial intrinsic heterogeneity of the enriched component in highly incompatible trace elements could also explain the subtle deviations from apparent two-component mixing lines for Icelandic samples in Pb–Pb isotope diagrams, which were previously thought to require more than two source components. In contrast to complete mixing (model 1A), incomplete mixing of melts and extraction of these mixtures from variable depths (model 2) reproduces the observed variability in trace element and Pb–Hf–Nd–Sr isotope compositions for Icelandic lavas, even if a constant ratio of the enriched and depleted source component (3:97) is assumed. Two components in the mantle source beneath Iceland therefore suffice to explain the large range in compositional variability observed in post-glacial lavas.

The example of Iceland demonstrates that melt mixing during melting of a heterogeneous mantle source is a key process for controlling the trace element and isotopic variability of oceanic basalts in general. For accurately inferring the presence of multiple source components from global MORB or OIB data, melt mixing during extraction from the mantle must be evaluated.

ACKNOWLEDGEMENTS

We are grateful to John Maclennan for his enthusiasm and help during sample collection in Iceland and the good discussions at a later stage. Tim Elliott is also thanked for helpful comments and discussions. Garett Ito and two anonymous reviewers are thanked for their constructive reviews, which led to great improvement of the paper. Gerhard Wörner is thanked for the editorial handling and helpful comments.

FUNDING

The study was funded by the Swiss National Science Foundation (SNSF grant 200020.121985 and 200021.113625).

SUPPLEMENTARY DATA

Supplementary data for this paper are available at *Journal of Petrology* online.

REFERENCES

Aigner-Torres, M., Blundy, J., Ulmer, P. & Pettke, T. (2007). Laser ablation ICPMS study of trace element partitioning between plagioclase and basaltic melts: an experimental approach. *Contributions to Mineralogy and Petrology* **153**, 647–667.

Allen, R. M., Nolet, G., Morgan, W. J., Vogfjord, K., Bergsson, B. H., Erlendsson, P., Foulger, G. R., Jakobsdottir, S., Julian, B. R., Pritchard, M., Ragnarsson, S. & Stefansson, R. (2002). Imaging the mantle beneath Iceland using integrated seismological techniques. *Journal of Geophysical Research, Solid Earth* **107**, 2325, doi:10.1029/2001JB000595.

Arevalo, R., Jr & McDonough, W. F. (2010). Chemical variations and regional diversity observed in MORB. *Chemical Geology* **271**, 70–85.

Asimow, P. D., Dixon, J. E. & Langmuir, C. H. (2004). A hydrous melting and fractionation model for mid-ocean ridge basalts:

Application to the Mid-Atlantic Ridge near the Azores. *Geochemistry, Geophysics, Geosystems* **5**, Q01E16, doi:10.1029/2003gc000568.

Ayers, J. C., Dittmer, S. K. & Layne, G. D. (1997). Partitioning of elements between peridotite and H_2O at 2·0–3·0 GPa and 900–1100°C, and application to models of subduction zone processes. *Earth and Planetary Science Letters* **150**, 381–398.

Beattie, P. (1994). Systematics and energetics of trace-element partitioning between olivine and silicate melts—implications for the nature of mineral melt partitioning. *Chemical Geology* **117**, 57–71.

Beier, C., Stracke, A. & Haase, K. M. (2007). The peculiar geochemical signatures of São Miguel (Azores) lavas: Metasomatised or recycled mantle sources? *Earth and Planetary Science Letters* **259**, 186–199.

Bijwaard, H. & Spakman, W. (1999). Tomographic evidence for a narrow whole mantle plume below Iceland. *Earth and Planetary Science Letters* **166**, 121–126.

Bindeman, I., Gurenko, A., Sigmarsson, O. & Chaussidon, M. (2008). Oxygen isotope heterogeneity and disequilibria of olivine crystals in large volume Holocene basalts from Iceland: Evidence for magmatic digestion and erosion of Pleistocene hyaloclastites. *Geochimica et Cosmochimica Acta* **72**, 4397–4420.

Bizzarro, M., Baker, J. A. & Ulfbeck, D. (2003). A new digestion and chemical separation technique for rapid and highly reproducible determination of Lu/Hf and Hf isotope ratios in geological materials by MC-ICP-MS. *Geostandards Newsletter* **27**, 133–145.

Blichert-Toft, J. & Albarède, F. (1997). The Lu–Hf isotope geochemistry of chondrites and the evolution of the mantle–crust system. *Earth and Planetary Science Letters* **148**, 243–258.

Blichert-Toft, J., Agranier, A., Andres, M., Kingsley, R., Schilling, J. G. & Albarède, F. (2005). Geochemical segmentation of the Mid-Atlantic Ridge north of Iceland and ridge–hot spot interaction in the North Atlantic. *Geochemistry, Geophysics, Geosystems* **6**, Q01E19, doi:10.1029/2004gc000788.

Bourdon, B., Ribe, N. M., Stracke, A., Saal, A. E. & Turner, S. P. (2006). Insights into the dynamics of mantle plumes from uranium-series geochemistry. *Nature* **444**, 713–717.

Carmichael, I. S. E. (1964). The petrology of Thingmuli, a Tertiary volcano in eastern Iceland. *Journal of Petrology* **5**, 435–460.

Chauvel, C. & Hémond, C. (2000). Melting of a complete section of recycled oceanic crust: Trace element and Pb isotopic evidence from Iceland. *Geochemistry, Geophysics, Geosystems* **1**, doi:10.1029/1999GC000002.

Chu, N. C., Taylor, R. N., Chavagnac, V., Nesbitt, R. W., Boella, R. M., Milton, J. A., German, C. R., Bayon, G. & Burton, K. (2002). Hf isotope ratio analysis using multi-collector inductively coupled plasma mass spectrometry: an evaluation of isobaric interference corrections. *Journal of Analytical Atomic Spectrometry* **17**, 1567–1574.

Eiler, J. M., Gronvold, K. & Kitchen, N. (2000). Oxygen isotope evidence for the origin of chemical variations in lavas from Theistareykir volcano in Iceland's northern volcanic zone. *Earth and Planetary Science Letters* **184**, 269–286.

Eiler, J. M., Farley, K. A., Valley, J. W., Hauri, E., Craig, H., Hart, S. R. & Stolper, E. M. (1997). Oxygen isotope variations in ocean island basalt phenocrysts. *Geochimica et Cosmochimica Acta* **61**, 2281–2293.

Elliott, T. R., Hawkesworth, C. J. & Gronvold, K. (1991). Dynamic melting of the Iceland plume. *Nature* **351**, 201–206.

Fitton, J. G., Saunders, A. D., Norry, M. J., Hardarson, B. S. & Taylor, R. N. (1997). Thermal and chemical structure of the Iceland plume. *Earth and Planetary Science Letters* **153**, 197–208.

Gautason, B. & Muehlenbachs, K. (1998). Oxygen isotopic fluxes associated with high-temperature processes in the rift zones of Iceland. *Chemical Geology* **145**, 275–286.

Gee, M. A. M., Taylor, R. N., Thirlwall, M. F. & Murton, B. J. (1998*a*). Glacioisostacy controls chemical and isotopic characteristics of tholeiites from the Reykjanes peninsula, SW Iceland. *Earth and Planetary Science Letters* **164**, 1–5.

Gee, M. A. M., Thirlwall, M. F., Taylor, R. N., Lowry, D. & Murton, B. J. (1998*b*). Crustal processes: Major controls on Reykjanes Peninsula lava chemistry, SW Iceland. *Journal of Petrology* **39**, 819–839.

Gurenko, A. A. & Chaussidon, M. (1995). Enriched and depleted primitive melts included in olivine from Icelandic tholeiites—origin by continuous melting of a single mantle column. *Geochimica et Cosmochimica Acta* **59**, 2905–2917.

Gurenko, A. A. & Sobolev, A. V. (2006). Crust–primitive magma interaction beneath neovolcanic rift zone of Iceland recorded in gabbro xenoliths from Midfell, SW Iceland. *Contributions to Mineralogy and Petrology* **151**, 495–520.

Hanan, B. B. & Graham, D. W. (1996). Lead and helium isotope evidence from oceanic basalts for a common deep source of mantle plumes. *Science* **272**, 991–995.

Hanan, B. B. & Schilling, J. G. (1997). The dynamic evolution of the Iceland mantle plume: the lead isotope perspective. *Earth and Planetary Science Letters* **151**, 43–60.

Hanan, B. B., Blichert-Toft, J., Kingsley, R. & Schilling, J. G. (2000). Depleted Iceland mantle plume geochemical signature: Artifact of multicomponent mixing? *Geochemistry, Geophysics, Geosystems* **1**, 1003, doi:10.1029/1999GC000009.

Hart, S. R. (1993). Equilibration during mantle melting—A fractal tree model. *Proceedings of the National Academy of Sciences of the USA* **90**, 11914–11918.

Hart, S. R. & Dunn, T. (1993). Experimental Cpx–melt partitioning of 24 trace-elements. *Contributions to Mineralogy and Petrology* **113**, 1–8.

Hart, S. R., Schilling, J. G. & Powell, J. L. (1973). Basalts from Iceland and along Reykjanes Ridge—Sr isotope geochemistry. *Nature, Physical Science* **246**, 104–107.

Hart, S. R., Hauri, E. H., Oschmann, L. A. & Whitehead, J. A. (1992). Mantle plumes and entrainment—isotopic evidence. *Science* **256**, 517–520.

Hart, S. R., Blusztajn, J., Dick, H. J. B., Meyer, P. S. & Muehlenbachs, K. (1999). The fingerprint of seawater circulation in a 500-meter section of ocean crust gabbros. *Geochimica et Cosmochimica Acta* **63**, 4059–4080.

Hémond, C., Arndt, N. T., Lichtenstein, U., Hofmann, A. W., Oskarsson, N. & Steinthorsson, S. (1993). The heterogeneous Iceland plume—Nd–Sr-O isotopes and trace-element constraints. *Journal of Geophysical Research, Solid Earth* **98**, 15833–15850.

Hermann, J., Spandler, C., Hack, A. & Korsakov, A. V. (2006). Aqueous fluids and hydrous melts in high-pressure and ultra-high pressure rocks: Implications for element transfer in subduction zones. *Lithos* **92**, 399–417.

Hirschmann, M. M., Asimow, P. D., Ghiorso, M. S. & Stolper, E. M. (1999). Calculation of peridotite partial melting from thermodynamic models of minerals and melts. III. Controls on isobaric melt production and the effect of water on melt production. *Journal of Petrology* **40**, 831–851.

Hirschmann, M. M., Kogiso, T., Baker, M. B. & Stolper, E. M. (2003). Alkalic magmas generated by partial melting of garnet pyroxenite. *Geology* **31**, 481–484.

Hofmann, A. W. (1988). Chemical differentiation of the Earth—the relationship between mantle, continental crust, and oceanic crust. *Earth and Planetary Science Letters* **90**, 297–314.

Ito, E., White, W. M. & Gopel, C. (1987). The O, Sr, Nd and Pb isotope geochemistry of MORB. *Chemical Geology* **62**, 157–176.

Ito, G. & Mahoney, J. J. (2005). Flow and melting of a heterogeneous mantle: 1. Method and importance to the geochemistry of ocean island and mid-ocean ridge basalts. *Earth and Planetary Science Letters* **230**, 29–46.

Ito, G., Shen, Y., Hirth, G. & Wolfe, C. J. (1999). Mantle flow, melting, and dehydration of the Iceland mantle plume. *Earth and Planetary Science Letters* **165**, 81–96.

Jakobsson, S. P. (1972). Chemistry and distribution pattern of recent basaltic rocks in Iceland. *Lithos* **5**, 365–386.

Jakobsson, S. P., Jonsson, J. & Shido, F. (1978). Petrology of the Western Reykjanes Peninsula, Iceland. *Journal of Petrology* **19**, 669–705.

Johnson, M. C. & Plank, T. (1999). Dehydration and melting experiments constrain the fate of subducted sediments. *Geochemistry, Geophysics, Geosystems* **1**, 1007, doi:10.1029/1999GC000014.

Jull, M. & McKenzie, D. (1996). The effect of deglaciation on mantle melting beneath Iceland. *Journal of Geophysical Research, Solid Earth* **101**, 21815–21828.

Kaban, M. K., Flóvenz, Ó. G. & Pálmason, G. (2002). Nature of the crust–mantle transition zone and the thermal state of the upper mantle beneath Iceland from gravity modelling. *Geophysical Journal International* **149**, 281–299.

Kempton, P. D., Fitton, J. G., Saunders, A. D., Nowell, G. M., Taylor, R. N., Hardarson, B. S. & Pearson, G. (2000). The Iceland plume in space and time: a Sr–Nd–Pb–Hf study of the North Atlantic rifted margin. *Earth and Planetary Science Letters* **177**, 255–271.

Kitagawa, H., Kobayashi, K., Makishima, A. & Nakamura, E. (2008). Multiple pulses of the mantle plume: evidence from Tertiary Icelandic lavas. *Journal of Petrology* **49**, 1365–1396.

Klimm, K., Blundy, J. D. & Green, T. H. (2008). Trace element partitioning and accessory phase saturation during H_2O-saturated melting of basalt with implications for subduction zone chemical fluxes. *Journal of Petrology* **49**, 523–553.

Kogiso, T., Tatsumi, Y. & Nakano, S. (1997). Trace element transport during dehydration processes in the subducted oceanic crust: 1. Experiments and implications for the origin of ocean island basalts. *Earth and Planetary Science Letters* **148**, 193–205.

Kogiso, T., Hirschmann, M. M. & Pertermann, M. (2004). High-pressure partial melting of mafic lithologies in the mantle. *Journal of Petrology* **45**, 2407–2422.

Kokfelt, T. F., Hoernle, K. & Hauff, F. (2003). Upwelling and melting of the Iceland plume from radial variation of ^{238}U–^{230}Th disequilibria in post-glacial volcanic rocks. *Earth and Planetary Science Letters* **214**, 167–186.

Kokfelt, T. F., Hoernle, K., Hauff, F., Fiebig, J., Werner, R. & Garbe-Schoenberg, D. (2006). Combined traced element and Pb–Nd–Sr–O isotope evidence for recycled oceanic crust (upper and lower) in the Iceland mantle plume. *Journal of Petrology* **47**, 1705–1749.

MacLennan, J. (2008*a*). Concurrent mixing and cooling of melts under Iceland. *Journal of Petrology* **49**, 1931–1953.

Maclennan, J. (2008*b*). Lead isotope variability in olivine-hosted melt inclusions from Iceland. *Geochimica et Cosmochimica Acta* **72**, 4159–4176.

Maclennan, J., Jull, M., McKenzie, D., Slater, L. & Gronvold, K. (2002). The link between volcanism and deglaciation in Iceland. *Geochemistry, Geophysics, Geosystems* **3**, 1062, doi:10.1029/2001GC000282.

Maclennan, J., McKenzie, D., Gronvold, K., Shimizu, N., Eiler, J. M. & Kitchen, N. (2003*a*). Melt mixing and crystallization under Theistareykir, northeast Iceland. *Geochemistry, Geophysics, Geosystems* **4**, 8624, doi:10.1029/2003gc000558.

Maclennan, J., McKenzie, D., Hilton, F., Gronvold, K. & Shimizu, N. (2003*b*). Geochemical variability in a single flow from northern Iceland. *Journal of Geophysical Research, Solid Earth* **108.**

McDonough, W. F. & Sun, S. S. (1995). The composition of the Earth. *Chemical Geology* **120**, 223–253.

McKenzie, D., Stracke, A., Blichert-Toft, J., Albarède, F., Gronvold, K. & O'Nions, R. K. (2004). Source enrichment processes responsible for isotopic anomalies in oceanic island basalts. *Geochimica et Cosmochimica Acta* **68**, 2699–2724.

Melekhova, E., Schmidt, M. W., Ulmer, P. & Pettke, T. (2007). The composition of liquids coexisting with dense hydrous magnesium silicates at 11–13·5 GPa and the endpoints of the solidi in the MgO–SiO_2–H_2O system. *Geochimica et Cosmochimica Acta* **71**, 3348–3360.

Montelli, R., Nolet, G., Masters, G., Dahlen, F. A. & Hung, S. H. (2004). Global P and PP traveltime tomography: rays versus waves. *Geophysical Journal International* **158**, 637–654.

Münker, C., Weyer, S., Scherer, E. & Mezger, K. (2001). Separation of high field strength elements (Nb, Ta, Zr, Hf) and Lu from rock samples for MC-ICPMS measurements. *Geochemistry, Geophysics, Geosystems* **2**, 1064, doi:10.1029/2001GC000183.

Nicholson, H., Condomines, M., Fitton, J. G., Fallick, A. E., Gronvold, K. & Rogers, G. (1991). Geochemical and isotopic evidence for crustal assimilation beneath Krafla, Iceland. *Journal of Petrology* **32**, 1005–1020.

Niu, Y. L. & Batiza, R. (1997). Trace element evidence from seamounts for recycled oceanic crust in the eastern Pacific mantle. *Earth and Planetary Science Letters* **148**, 471–483.

Oskarsson, N., Steinthorsson, S. & Sigvaldason, G. E. (1985). Iceland geochemical anomaly—origin, volcanotectonics, chemical fractionation and isotope evolution of the crust. *Journal of Geophysical Research, Solid Earth and Planets* **90**, 11–25.

Peate, D., Baker, J., Jakobsson, S., Waight, T., Kent, A., Grassineau, N. & Skovgaard, A. (2009). Historic magmatism on the Reykjanes Peninsula, Iceland: a snap-shot of melt generation at a ridge segment. *Contributions to Mineralogy and Petrology* **157**, 359–382.

Peate, D. W., Breddam, K., Baker, J. A., Kurz, M. D., Barker, A. K., Prestvik, T., Grassineau, N. & Skovgaard, A. C. (2010). Compositional characteristics and spatial distribution of enriched Icelandic mantle components. *Journal of Petrology* **51**, 1447–1475.

Pertermann, M. & Hirschmann, M. M. (2003). Partial melting experiments on a MORB-like pyroxenite between 2 and 3 GPa: Constraints on the presence of pyroxenite in basalt source regions from solidus location and melting rate. *Journal of Geophysical Research, Solid Earth* **108.**

Phipps Morgan, J. (1999). Isotope topology of individual hotspot basalt arrays: Mixing curves or melt extraction trajectories? *Geochemistry, Geophysics, Geosystems* **1**, 1003, doi:10.1029/1999GC000004.

Pin, C. & Zalduegui, J. F. S. (1997). Sequential separation of light rare-earth elements, thorium and uranium by miniaturized extraction chromatography: Application to isotopic analyses of silicate rocks. *Analytica Chimica Acta* **339**, 79–89.

Putirka, K. D. (2005). Mantle potential temperatures at Hawaii, Iceland, and the mid-ocean ridge system, as inferred from olivine phenocrysts: Evidence for thermally driven mantle plumes. *Geochemistry, Geophysics, Geosystems* **6**, Q05108, doi:10.1029/2005gc000915.

Regelous, M., Hofmann, A. W., Abouchami, W. & Galer, S. J. G. (2003). Geochemistry of lavas from the Emperor Seamounts, and the geochemical evolution of Hawaiian magmatism from 85 to 42 Ma. *Journal of Petrology* **44**, 113–140.

Ribe, N. M., Christensen, U. R. & Theissing, J. (1995). The dynamics of plume–ridge interaction. 1. Ridge-centered plumes. *Earth and Planetary Science Letters* **134**, 155–168.

Salters, V. J. M. & Stracke, A. (2004). Composition of the depleted mantle. *Geochemistry, Geophysics, Geosystems* **5**, Q05004, doi:10.1029/02003GC000597.

Salters, V. J. M. & White, W. M. (1996). Hf isotope constraints on mantle evolution. In: *Workshop on Geochemical Earth Reference Model, Lyon, France*. Amsterdam: Elsevier, pp. 447–460.

Schilling, J. (1973). Iceland mantle plume—geochemical study of Reykjanes Ridge. *Nature* **242**, 565–571.

Shen, Y., Solomon, S. C., Bjarnason, I. T. & Wolfe, C. J. (1998). Seismic evidence for a lower-mantle origin of the Iceland plume. *Nature* **395**, 62–65.

Sigmarsson, O., Condomines, M. & Fourcade, S. (1992*a*). A detailed Th, Sr and O isotope study of Hekla—differentiation processes in an Icelandic volcano. *Contributions to Mineralogy and Petrology* **112**, 20–34.

Sigmarsson, O., Condomines, M. & Fourcade, S. (1992*b*). Mantle and crustal contribution in the genesis of Recent basalts from off-rift zones in Iceland: Constraints from Th, Sr and O isotopes. *Earth and Planetary Science Letters* **110**, 149–162.

Sinton, J., Grönvold, K. & Sæmundsson, K. (2005). Postglacial eruptive history of the Western Volcanic Zone, Iceland. *Geochemistry, Geophysics, Geosystems* **6**, Q12009, doi:12010.11029/12005GC001021.

Skovgaard, A. C., Storey, M., Baker, J., Blusztajn, J. & Hart, S. R. (2001). Osmium-oxygen isotopic evidence for a recycled and strongly depleted component in the Iceland mantle plume. *Earth and Planetary Science Letters* **194**, 259–275.

Slater, L., McKenzie, D. A. N., Gronvold, K. & Shimizu, N. (2001). Melt generation and movement beneath Theistareykir, NE Iceland. 321–354.

Stoll, B., Jochum, K. P., Herwig, K., Amini, M., Flanz, M., Kreuzburg, B., Kuzmin, D., Willbold, M. & Enzweiler, J. (2008). An automated iridium-strip heater for LA-ICP-MS bulk analysis of geological samples. *Geostandards and Geoanalytical Research* **32**, 5–26.

Stracke, A. & Bourdon, B. (2009). The importance of melt extraction for tracing mantle heterogeneity. *Geochimica et Cosmochimica Acta* **73**, 218–238.

Stracke, A., Bizimis, M. & Salters, V. J. M. (2003*a*). Recycling oceanic crust: Quantitative constraints. *Geochemistry, Geophysics, Geosystems* **4**, 8003, doi:10.1029/2001GC000223.

Stracke, A., Bourdon, B. & McKenzie, D. (2006). Melt extraction in the Earth's mantle: Constraints from U–Th–Pa–Ra studies in oceanic basalts. *Earth and Planetary Science Letters* **244**, 97–112.

Stracke, A., Hofmann, A. W. & Hart, S. R. (2005). FOZO, HIMU, and the rest of the mantle zoo. *Geochemistry, Geophysics, Geosystems* **6**, Q05007, doi:10.01029/02004gc000824.

Stracke, A., Salters, V. J. M. & Sims, K. W. W. (1999). Assessing the presence of garnet-pyroxenite in the mantle sources of basalts through combined hafnium–neodymium–thorium isotope systematics. *Geochemistry, Geophysics, Geosystems* **1**, 1006, doi:10.1029/1999GC000013.

Stracke, A., Zindler, A., Salters, V. J. M., McKenzie, D. & Grönvold, K. (2003*b*). The dynamics of melting beneath Theistareykir, northern Iceland. *Geochemistry, Geophysics, Geosystems* **4**, 8513, doi:10.1029/2002GC000347.

Stracke, A., Zindler, A., Salters, V. J. M., McKenzie, D., Blichert-Toft, J., Albarède, F. & Gronvold, K. (2003*c*). Theistareykir revisited. *Geochemistry, Geophysics, Geosystems* **4**, 8507, doi:10.1029/2001GC000201.

Su, Y. J. (2002). Mid-ocean ridge basalts trace element systematics: constraints from database management, ICP-MS analyses, global data compilation and petrologic modeling. New York: Columbia University, 472 p.

Sun, S.-S. & McDonough, W. F. (1989). Chemical and isotopic systematics of oceanic basalts: implications for mantle composition and processes. In: Norry, A. D. & Saunders, M. J. (eds) *Magmatism in the Ocean Basins. Geological Society, London, Special Publications* **42**, 313–345.

Sun, W., Hu, Y., Kamenetsky, V. S., Eggins, S. M., Chen, M. & Arculus, R. J. (2008). Constancy of Nb/U in the mantle revisited. *Geochimica et Cosmochimica Acta* **72**, 3542–3549.

Thirlwall, M. F., Gee, M. A. M., Taylor, R. N. & Murton, B. J. (2004). Mantle components in Iceland and adjacent ridges investigated using double-spike Pb isotope ratios. *Geochimica et Cosmochimica Acta* **68**, 361–386.

Thirlwall, M. F., Gee, M. A. M., Lowry, D., Mattey, D. P., Murton, B. J. & Taylor, R. N. (2006). Low $\delta^{18}O$ in the Icelandic mantle and its origins: Evidence from Reyjanes Ridge and Icelandic lavas. *Geochimica et Cosmochimica Acta* **70**, 993–1019.

Weis, D., Kieffer, B., Hanano, D., Silva, I. N., Barling, J., Pretorius, W., Maerschalk, C. & Mattielli, N. (2007). Hf isotope compositions of US Geological Survey reference materials. *Geochemistry, Geophysics, Geosystems* **8**, Q06006, doi:10.1029/02006gc001473.

Willbold, M. & Stracke, A. (2006). Trace element composition of mantle end-members: Implications for recycling of oceanic and upper and lower continental crust. *Geochemistry, Geophysics, Geosystems* **7**, Q04004, doi:10.1029/02005gc001005.

Willbold, M. & Stracke, A. (2010). Formation of enriched mantle components by recycling of upper and lower continental crust. *Chemical Geology* **276**, 188–197.

Willbold, M., Hegner, E., Stracke, A. & Rocholl, A. (2009). Continental geochemical signatures in dacites from Iceland and implications for models of early Archaean crust formation. *Earth and Planetary Science Letters* **279**, 44–52.

Wolfe, C. J., Bjanason, I. Th., Vandecar, C. J. & Solomon, S. C. (1997). Seismic structure of the Iceland mantle plume. *Nature* **385**, 245–247.

Wood, D. A. (1981). Partial melting models for the petrogenesis of Reykjanes Peninsula Basalts, Iceland—implications for the use of trace-elements and strontium and neodymium isotope ratios to record inhomogeneities in the upper mantle. *Earth and Planetary Science Letters* **52**, 183–190.

Wood, D. A., Joron, J. L., Treuil, M., Norry, M. & Tarney, J. (1979). Elemental and Sr isotope variations in basic lavas from iceland and the surrounding ocean-floor—nature of mantle source inhomogeneities. *Contributions to Mineralogy and Petrology* **70**, 319–339.

Workman, R. K. & Hart, S. R. (2005). Major and trace element composition of the depleted MORB mantle (DMM). *Earth and Planetary Science Letters* **231**, 53–72.

Zindler, A. & Hart, S. (1986). Chemical geodynamics. 493–571.

Zindler, A., Staudigel, H. & Batiza, R. (1984). Isotope and trace-element geochemistry of young Pacific seamounts—implications for the scale of upper mantle heterogeneity. *Earth and Planetary Science Letters* **70**, 175–195.

Zindler, A., Hart, S. R., Frey, F. A. & Jakobsson, S. P. (1979). Nd and Sr isotope ratios and rare-earth element abundances in Reykjanes Peninsula basalts—evidence for mantle heterogeneity beneath Iceland. *Earth and Planetary Science Letters* **45**, 249–262.